Prabha Materials Science Letters
Vol. 5, No. 1, 123-158, 2026
https://doi.org/10.33889/PMSL.2026.5.1.007

Non-Catalytic Hydrogen Abstraction Kinetics of Aldehyde–Methyl Radical Reactions: A DFT Benchmark Perspective

Yuvarani Sambathkumar
Department of Physics,
PSGR Krishnammal College for Women, Coimbatore, Tamil Nadu, India.
E-mail: syuva2987@gmail.com

Abiram Angamuthu
Department of Physics,
Rathinam Technical Campus, Coimbatore, Tamil Nadu, India.
E-mail: aabiram@gmail.com

Praveena Gopalan
Department of Physics,
PSGR Krishnammal College for Women, Coimbatore, Tamil Nadu, India.
Corresponding author: praveenag@psgrkcw.ac.in

(Received on December 20, 2025; Revised on January 18, 2026 & January 19, 2026; Accepted on February 8, 2026)

Abstract
Hydrogen abstraction plays a key role in the atmospheric oxidation of aldehydes and halogenated aldehydes. Their reactivity with atmospheric radicals determines the transformation mechanisms and contribution to secondary pollutant formation, which is essential for evaluating their environmental behavior. The primary objective of this study is to benchmark the performance of three density functionals–B3LYP, M06-2X, and ωB97X-D across three basis set combinations (6-311+G(d,p), 6-311++G(d,p) and 6-311++G(2d,2p)) in predicting the non-catalytic H-abstraction reactions of substituted aldehydes (XCHO, where X = CH_3, CF_3, CCl_3, H, F, Cl) in the presence of methyl radical ($\dot{C}H_3$). The rate constants were computed using conventional transition state theory (TST) with Eckart tunnelling effect over a temperature range of 300-1700 K. The accuracy of each functional is evaluated by comparing the reaction energies, transition states, thermochemical properties and rate constants obtained in both gas and water-mediated environments with the available experimental and high-level theoretical data. The meta-hybrid GGA functional, M06-2X with better electron correlation and electron density localization effects consistently outperformed others in predicting the barrier energies, reaction enthalpies and rate constants. Also, in addition to M06-2X, the range-separated (RS) hybrid GGA functional ωB97X-D showed reasonable accuracy for rate constants at elevated temperatures (1300-1700 K), while B3LYP underestimated barrier energies and overestimated the rate constants. Among the chosen aldehydes, the aldehydic H-abstraction of ClCHO and CH_3CHO exhibited the most favourable paths, while FCHO and H-abstraction from methyl site of CH_3CHO took least favourable routes across the temperature range. The benchmarking of the considered H-abstraction reactions in general highlights the interplay between the choice of functionals, basis-sets and substituent-driven electronic effects in predicting reaction barriers and rate constants.

Keywords- DFT functionals, H-abstraction reaction, Aldehydes and halogenated aldehydes, Methyl radical, Rate coefficients, Transition state theory, Temperature-dependent kinetics.

1. Introduction

Abstraction reaction is a key step in atmospheric oxidation of organic molecules that initiates the breakdown to form radicals that undergo subsequent reactions resulting in the formation of secondary pollutants (Atkinson and Arey, 2003). Hydrogen abstraction (H- abstraction), a widely studied pathway, is fundamental to hydrocarbon combustion and atmospheric oxidation of volatile organic compounds (VOCs) (Basch and Hoz, 1997) that are influenced by bond strengths of C-H bonds, radical stability, and environmental conditions. Among the various compound abstraction reactions, the H- abstraction

reactions of halogenated aldehydes stand out due to their unique environmental significance in atmospheric chemistry (Carr et al., 2003). These reactions play a key role as sinks in determining the atmospheric lifetime and transformation pathways of these compounds (Doherty and Carpenter, 2007).

Halogenated molecules such as fluorinated (CH_3CFH_2) (Wallington et al., 1992; Hasson et al., 1998) and chlorinated (CH_2Cl, $CHCl_3$) (Sanhueza and Heicklen, 1975; Niki et al., 1980) hydro chlorofluorocarbons (HCFCs) (Wallington et al., 2017) are some of the important intermediates in the atmospheric degradation process. These compounds serve as the carriers of halogens into the stratosphere (Hubrich and Stuhl, 1980; Doherty and Carpenter, 2007) causing ozone depletion, (Montzka et al., 2011; Wilmouth et al., 2018) global warming (Dong et al., 2025) and changes in atmospheric oxidation capacity (Chen et al., 2024). The primary removal route of HCFCs from the atmosphere occurs via photolysis or radical oxidation as initiated by the abstraction process that lead to the formation of chlorinated and fluorinated carbonyls and acids (Kelly et al., 2005; Chiappero et al., 2006). Among several oxidants in the chemistry of abstraction reactions, due to its high reactivity and constant tropospheric concentration of about $9.7x10^5$ radicals cm^{-3}, the hydroxyl radical oxidant plays an important role in the atmospheric degradation (Kovacevic & Sabljic, 2017). Additionally, other atmospheric oxidants such as ozone (O_3), the nitrate radical (NO_x), hydroperoxyl radicals (HO_2), methyl radical (CH_3), cyano radical (CN) and halogen atoms also contribute to the removal of anthropogenic pollutants from the atmosphere.

Experimental and theoretical investigations on the H-abstraction reaction kinetics of aldehydes and substituted aldehydes in the presence of hydroxyl radical (OH), (Kerr and Sheppard, 1981; Mora-Diez et al., 2001) nitrogen oxides (NOx), (Mora-Diez and Boyd, 2002) and chlorine (Cl) (Beukes et al., 2000) oxidants are available. Scollard et al. (1993) investigated H- abstraction rates of halogenated aldehydes CX_3CHO (X = H, Cl or F) with OH and Cl radicals at 298K using pulsed laser photolysis. Their findings show that halogen substitution reduces reactivity with rate constants of 10^{-12} to 10^{-13} cm^3 $molecule^{-1}$ s^{-1} for OH and 10^{-11} to 10^{-12} cm^3 $molecule^{-1}$ s^{-1} for Cl radicals, in contrast to the typical value of 10^{-11} cm^3 $molecule^{-1}$ s^{-1} for non-halogenated aldehydes. Farahani et al. (2015) studied the reaction mechanism of halo methane (CH_3Cl, CF_3Cl, CH_3Br and CF_3Br) with cyano radicals and reported that the lower barrier pathway for H- abstraction occurs through cyano-carbon with the rate constant of $1.21x10^{-13}$ cm^3 $molcule^{-1}$ s^{-1}. Buszek et al. (2011) investigated the water-catalysed H- abstraction reaction of acetaldehyde by OH radical at 77K. The same reaction (CH_3CHO + OH) was also studied theoretically using ab initio methods (Vohringer-Martinez et al., 2007), where it is found that the addition of water lowers the activation energy by the order of about 7 kJ/mol.

Mora-Diez & Boyd (2002) provided a comparative analysis on the accuracy of different theoretical methods (MP2, MP4, B3LYP, BH&HLYP), revealing that MP2 and BH&HLYP combined with CCSD(T) level perform better than other hybrid methods for H- abstraction reactions of NO_3 with XCHO (where X = H, F, Cl and CH_3). A few other studies (Gao et al., 2020; Vijayakumar and Wilmouth, 2021) employed the M062X and MP2 functionals with an augmented correlation-consistent basis set for H-abstraction from 2-butanone and formyl chloride by OH and Cl radical. Cao et al. (2021) studied the reaction kinetics of the CH_3 radical with HOOH, CH_3OOH, and CH_3CH_2OOH using B3LYP, MP2, and M062X methods.

Most of the above studies highlight the accuracy of computationally expensive high-level electron correlation method such as MP2 in combination with CCSD(T) (Gao et al., 2020; Cao et al., 2021; Vijayakumar and Wilmouth, 2021; Zokaie et al., 2021) for determining reaction pathways and thermodynamic parameters. On the other hand, a wide range of density functional methods is available for studying the kinetics and mechanisms of atmospheric reactions, with different hybrid functionals

offering distinct advantages and limitations (Ma et al., 2018; Liu et al., 2025). In order to ensure the accuracy of such functionals compared to higher-level electron correlation methods, a benchmark evaluation of various DFT approaches for atmospheric reactions needs to be performed. However, most existing kinetic studies are limited to room temperature (298 K), leaving the temperature dependence of reaction rate constants largely unexplored (Scollard et al., 1993). To address these gaps, the present study provides a comprehensive benchmark in evaluating the accuracy of three density functionals—B3LYP (hybrid), M06-2X (hybrid meta-GGA), and ωB97X-D (range-separated hybrid)—for predicting the mechanisms and temperature dependent kinetics of non-catalytic H-abstraction reactions of aldehydes and halogenated aldehydes by the methyl radical ($\dot{C}H_3$).

Although $\dot{C}H_3$ is present at relatively low steady-state concentrations in the atmosphere, it is continuously formed through methane oxidation, biomass burning and photochemical processes. Owing to its high intrinsic reactivity across a wide temperature range, $\dot{C}H_3$ acts as a kinetically competitive radical in both atmospheric and combustion environments. In the atmospheric context, since water vapour is a major component of the troposphere, its inclusion via implicit solvation allows for the evaluation of solvation-induced effects on hydrogen abstraction mechanisms, particularly the stabilization of radical intermediates and their impact on activation free energies and temperature-dependent rate constants relative to gas-phase conditions. Accordingly, this study investigates the reactions of formaldehyde (HCHO), acetaldehyde (CH_3CHO), and a series of halogenated aldehydes such as formyl fluoride (FCHO), formyl chloride (ClCHO), trifluoroacetaldehyde (CF_3CHO), and trichloroacetaldehyde (CCl_3CHO) with the $\dot{C}H_3$ in both gas-phase and water-mediated environments using implicit solvation models. This approach enables the establishment of substituent-specific reactivity trends, determination of temperature-dependent rate constants with tunnelling corrections and provides mechanistic insight into aldehyde oxidation pathways relevant to atmospheric chemistry.

In particular, the novelty of this work lies in (i) providing a systematic DFT benchmark of non-catalytic hydrogen abstraction kinetics for aldehyde-methyl radical reactions, (ii) evaluating the basis-set dependence of transition-state energetics and rate constants, with special emphasis on diffuse and higher polarization functions, and (iii) offering a comparative kinetic perspective that is currently lacking in the literature, where most previous studies focus either on thermochemistry or on single-level kinetic estimates.

2. System Set-up and Computational Methodology

A computational benchmark of the density functionals such as B3LYP, M06-2X and ωB97X-D in predicting the temperature dependent kinetics of H-abstraction mechanisms of organic pollutants based on aldehydes (HCHO and CH_3CHO) and halogenated aldehydes (FCHO, ClCHO, CF_3CHO and CCl_3CHO) in the presence of $\dot{C}H_3$ is carried out. To provide a useful means to discriminate basis sets, a larger split-valence triple-zeta 6-311++G(2d,2p) basis set with diffuse functions and 6-311+G(d,p) and 6-311++G(d,p) basis sets with additional two sets of d-type and p-type polarization functions to the non-hydrogen and hydrogen species are employed in the study. Diffuse functions (+, ++) were included to accurately describe the delocalized electron density of open-shell radicals and pre-reactive complexes, while polarization functions (d,p)/(2d,2p) improve molecular geometries and activation barrier heights that directly control kinetic predictions. The uses of Pople-type triple-ζ quality basis sets provide a balanced compromise between accuracy and computational cost. These choices were selected primarily on the basis of established literature reports that demonstrated their reliability in describing radical kinetics and transition-state geometries and the need for an internal convergence assessment tailored to the present reaction system. The quantitative comparison of basis-set performance is presented in the

results and discussion section. Altogether three DFT functionals namely: B3LYP, (Lee et al., 1988) M06-2X (Mardirossian & Head-Gordon, 2016) and ωB97X-D (Chai and Head-Gordon, 2008) in conjunction with three basis sets: 6-311+G(d,p), 6-31++G(d,p) and 6-311++G(2d,2p) are used for the computation of H-abstraction reactions in both gas and water mediated environments.

Figure 1 illustrates the H-abstraction reaction mechanisms of interest. From the scheme, it is inferred that the reactive carbon center of $\dot{C}H_3$ initiates the reaction by forming pre-reactant complexes ($\dot{C}H_3\cdots XCHO$, where X = H, F, Cl, CH_3, CF_3, CCl_3). These complexes then precede through their respective transition states (activated complex) to form the product complexes that result finally into products.

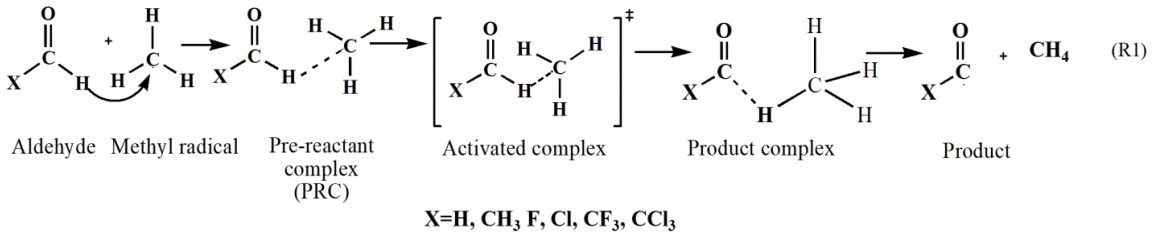

Figure 1. Schematic representation of hydrogen abstraction reaction.

Following the above outlined scheme (**Figure 1**), this study primarily focusses on a set of seven non-catalytic H-abstraction reactions of HCHO, CH_3CHO and XCHO (X = F, Cl, CF_3 & CCl_3) by $\dot{C}H_3$ as denoted by rn1-rn7 below. The selective removal of hydrogen atom is considered to be taken place by the reactive carbon atom ($\dot{C}$) of $\dot{C}H_3$. In order to understand the most probable H-removal site in acetaldehyde (CH_3CHO), H-abstraction is made to occur at two distinct sites namely: the aldehydic hydrogen (—CHO) and the methyl hydrogen (—CH_3) (refer reactions rn4 & rn5). However, as can be seen from **Figure 2**, the only available H-removal site of all the other aldehydes is the aldehydic hydrogen of the respective compounds.

$$HCHO + \dot{C}H_3 \rightarrow H\dot{C}O + CH_4 \quad \text{(rn1)}$$
$$FCHO + \dot{C}H_3 \rightarrow F\dot{C}O + CH_4 \quad \text{(rn2)}$$
$$ClCHO + \dot{C}H_3 \rightarrow Cl\dot{C}O + CH_4 \quad \text{(rn3)}$$
$$CH_3CHO + \dot{C}H_3 \rightarrow CH_3\dot{C}O + CH_4 \quad \text{(rn4)}$$
$$CH_3CHO + \dot{C}H_3 \rightarrow CH_2\dot{C}HO + CH_4 \quad \text{(rn5)}$$
$$CF_3CHO + \dot{C}H_3 \rightarrow CF_3\dot{C}O + CH_4 \quad \text{(rn6)}$$
$$CCl_3CHO + \dot{C}H_3 \rightarrow CCl_3\dot{C}O + CH_4 \quad \text{(rn7)}$$

The geometries of the reactants (R), pre-reactant complexes (PRC), transition states (TS), product complexes (PC) and products (P) of the above reactions (rn1-rn7) are optimized at nine levels of theories namely: B3LYP/6-311+G(d,p), B3LYP/6-311++G(d,p), B3LYP/6-311++G(2d,2p), M06-2X/6-311+G(d,p), M06-2X/6-311++G(d,p), M06-2X/6-311++G(2d,2p), ωB97X-D/6-311+G(d,p), ωB97X-D/6-311+G(d,p), ωB97X-D/6-311+G(d,p) and B3LYP/6-311+G(d,p) at standard temperature 298.15 K and pressure of 1atm in both gas and water phases. The harmonic vibrational frequencies of the optimized geometries of the (R), (PRC), (PC) and (P) account for the positive values with transition state structures (TS) characterized by one imaginary frequency. The optimization of the transition state is carried out

using Synchronous Transit-Guided Quasi-Newton (STQN) method (Peng and Schlegel Jr, 1993). In order to confirm the presence of TS along the reaction path connecting the reactants and products, the IRC calculations were performed using B3LYP/6-311+G(d,p), M06-2X/6-311+G(d,p) and ωB97X-D/6-311+G(d,p) levels of theory (Gonzalez and Schlegel, 1989). The optimized energies including the final electronic energy, Gibbs free energy and enthalpy of all the species at all the nine levels of theory are further subjected to zero-point energy corrections for the effective analyses of their thermodynamical functions. Solvent effects were included via an implicit water model to capture the stabilization of polar transition states and radical intermediates in hydrogen abstraction reactions. The implicit solvent effects were made by employing conductor-like polarizable continuum model (CPCM) using self-consistent reaction field (SCRF) approach (Tapia and Goscinski, 1975).

As this study mainly focusses on the temperature dependent kinetics, the rate constants for all the considered reactions were calculated using conventional transition state theory (TST), (Truhlar and Pliego, 2006) which relates the temperature dependence of the rate constant to the properties of the transition state as,

$$k(T) = \frac{k_B T}{h} \frac{Q_{X^{\ddagger}}}{Q_A(T) Q_B(T)} exp\left(-\frac{V_a^{G^{\ddagger}}}{RT}\right) \quad (1)$$

where, h is the Planck's constant, k_B is the Boltzmann's constant, T is the temperature (300-1700K), $Q_{X^{\ddagger}}$ is the partition function for the transition state, $V_a^{G^{\ddagger}}$ is the energy barrier and $Q_A(T)$ *and* $Q_B(T)$ represent the partition functions of the reactants A and B respectively. In addition to calculating the conventional reaction rate, tunneling effects must be considered to account the quantum nature of the subatomic particles. Tunneling probability is governed by the mass of the migrating atom, the height and width of the energy barrier, making it a critical factor in determining the reaction kinetics involving hydrogen atom. The corrected tunneling reaction rate is given by,

$$k^X(T) = \kappa^x(T) k(T) \quad (2)$$

where, '$\kappa^x(T)$' can be one of three tunneling effects used such as Eckart (1930), Wigner (1932) and small curvature tunneling (SCT) (Fernández-Ramos et al., 2006). To better account for barrier shape and asymmetry, the Eckart tunneling model that employs an analytical one-dimensional potential with accurate tunneling probabilities for reactions and well-defined transition states is considered in the present study (Espinosa-García et al., 1994; Ma and Li, 2025). Rate constant calculations are performed using KiSThelp 2019 program package, (Canneaux et al., 2014) incorporating Eckart transmission coefficients derived from forward and reverse barrier heights, imaginary frequencies, and effective reduced masses along the reaction coordinate. This approach provides a balance between computational efficiency and mechanistic accuracy for predominantly one-dimensional reaction pathways. All the structural and thermodynamical calculations are performed using G09w program (Frisch, 2010).

3. Results and Discussion

3.1 Structural Variation of Reaction Species

The optimized geometries of R, PRC, TS, PC and P for the species involved in the reactions (rn1-rn7) obtained at M06-2X/6-311++G(2d,2p) level of theory in gas phase are displayed in **Figures 2 (1-2)** and **3**.

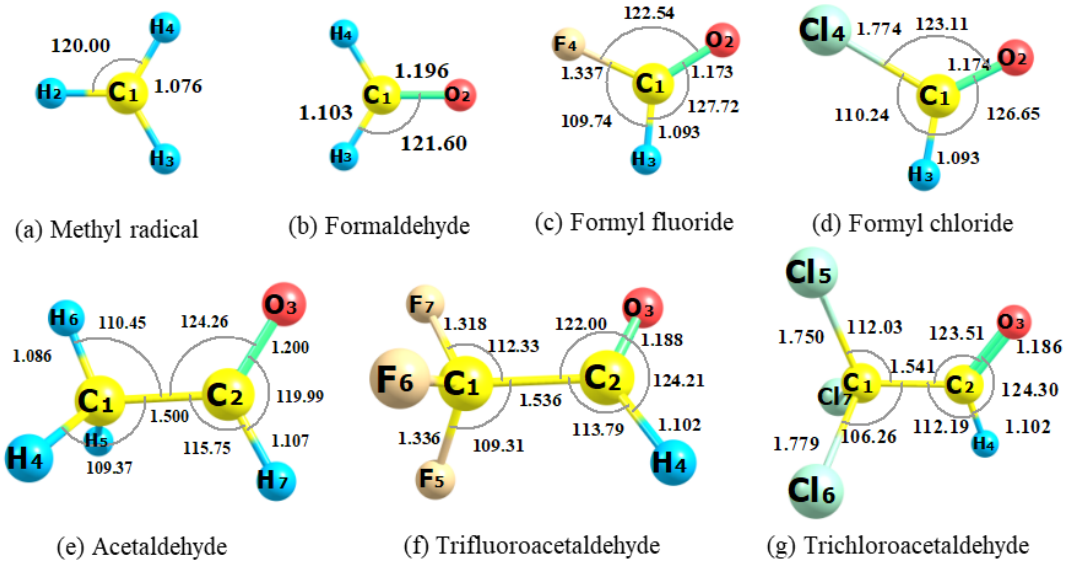

(1)

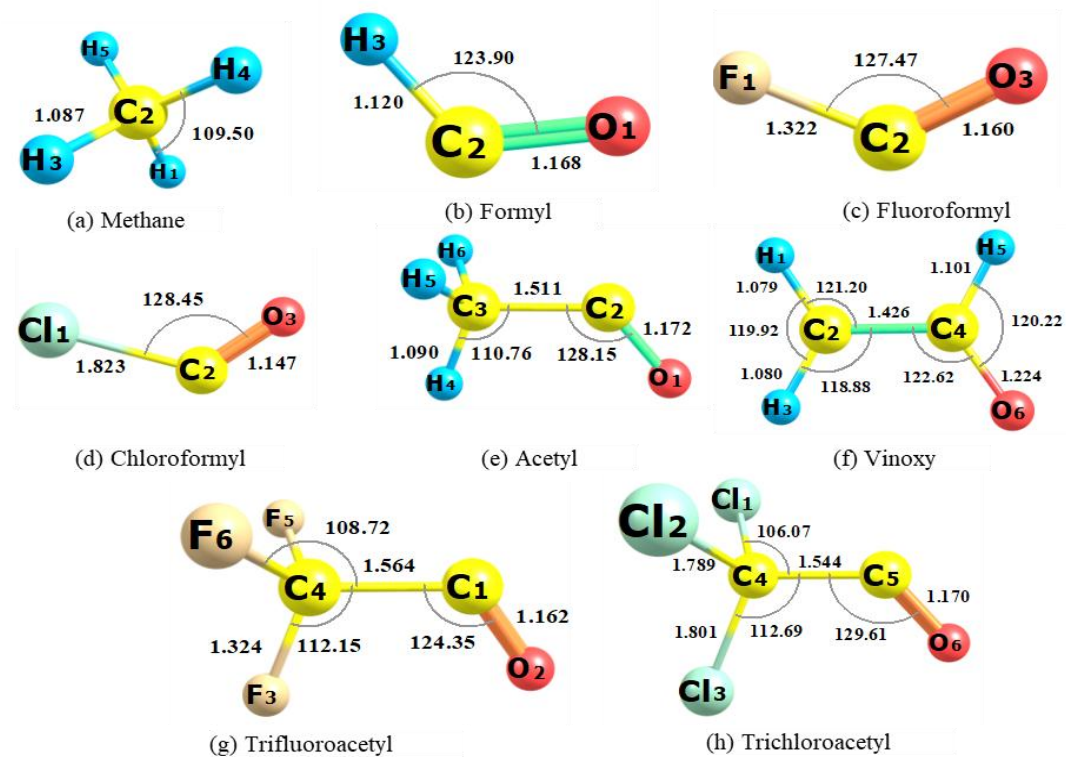

(2)

Figure 2. (1) Optimized geometries of the reactants calculated at M06-2X/6-311++G(2d,2p) level of theory. **(2)** Optimized geometries of the products calculated at M06-2X/6-311++G(2d,2p) level of theory.

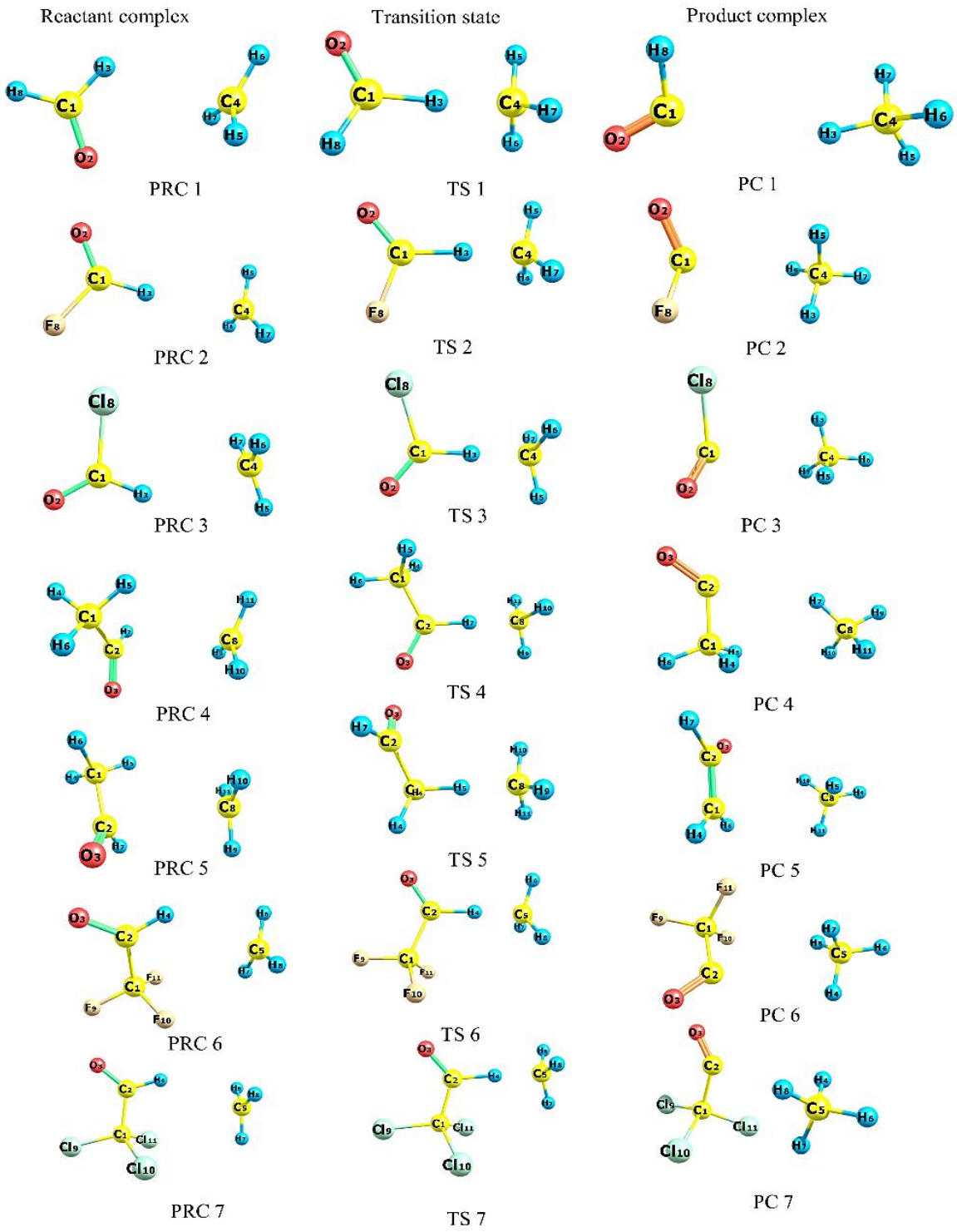

Figure 3. Optimized geometries for the species involved in the hydrogen abstraction reaction from XCHO (X = H, F, Cl, CF_3, CCl_3) by $\dot{C}H_3$ (rn1, rn2, rn3, rn4, rn5, rn6 and rn7) in gas phase obtained at M06-2X/6-311++G(2d,2p) level of theory.

The bond lengths and bond angles of the isolated reactants and products (CH_3, HCHO, FCHO, ClCHO, CH_3CHO, CF_3CHO, CCl_3CHO, HCO and CH_4) calculated using B3LYP, ωB97X-D and M06-2X functionals in conjunction with 6-311+G(d,p), 6-311++G(d,p) and 6-311++G(2d,2p) basis sets are compared with the available literature (refer **Tables S1** and **S2**). From tables, we found that the obtained values are almost in good accordance with available data with utmost deviation of less than 0.02 Å for bond lengths and not more than ±2° for bond angles.

The key structural parameters (C···H bond length and H-C-H bond angles) of the corresponding TS (TS1-TS7) geometries computed at all nine levels of theory in both gas and water phases are listed in the **Tables S3** and **S4**. For the gas phase abstractions (rn1-rn7), the C-H bond (for the corresponding substituent) of carbonyl group in PRC remains relatively consistent across the methods used. The variation in C-H bond lengths between the reactant complex and transition state reflects the degree of bond activation and nature of the transition state. The reaction proceeds via a transition state in which the hydrogen atom from carbonyl carbon (CHO) of the aldehydes (donor) is transferred to the methyl radical (abstracting radical), forming a new C···H bond at the radical site. This further in-turn results in the generation of a carbon-centered radical at the donor molecule, which remains as a reactive intermediate following H- abstraction. The C···H bond lengths in TS geometry is found to be slightly influenced by both the nature of the substituents (X = H, F, Cl, CH_3, CF_3 and CCl_3) and the choice of functionals used (refer **Table S3**). Notably in the presence of electron withdrawing groups (X = F, CF_3 and CCl_3), the bond associated with the elongation of C-H at the aldehydic site is longer and is more pronounced in FCHO (TS2) (1.33Å). Whereas, the bond associated with the formation of C···H at the radical site shows shorter C···H distance (~1.37Å) in FCHO with respect to other substituents. This geometry of TS (**Figure 3** (TS 2)) as a consequence of inductive electron withdrawing effects might indicate a more product like structure delaying the formation of product with higher activation barrier.

Further, in the reaction mechanism rn1, the shortest bond associated with C-H formation (1.470Å) is obtained using ωB97X-D/6-311++G(2d,2p) method indicating a better treatment of dispersion and long-range effects. In contrast, B3LYP/6-311++G(d,p) gives the longest bond length of about 1.493Å, while M06-2X/6-311++G(d,p) gives an intermediate value (1.482 Å). This reflects the importance of Hartree-Fock exchange with medium-range correlation and dispersion corrections in the M06-2X and ωB97X-D functionals and further reflects the limited treatment of long-range correlation in B3LYP functional. From the transition state geometry leading to dissociation, it observed that the M06-2X functional predicts the shortest C-H bond distance of the order of 1.266Å with ωB97X-Dand B3LYP functionals predicting slightly longer bond lengths of 1.272Å and 1.274 Å. This shows a better treatment of tighter transition states and stronger orbital interaction by M06-2X functional, while ωB97X-D and B3LYP functionals predict slightly delocalized and looser TS. Almost a comparable trend in the formation and elongation of C-H bond length is observed for all the reactions (rn2-rn7).

3.2 Reaction Pathways for H- Abstraction Reactions

Figures 4(1) and **4(2)** show the potential energy surface (PES) with relative energies (ΔE) of the constituents to those of their corresponding reactants in gas and water phase. The relative energies for all intermediate species and transition states are listed in **Tables S5** and **S6**. From **Table S5**, we infer that the PRCs of (rn1-rn7) computed by B3LYP functional exhibit relatively weaker ΔE that are lesser by about 1.5-2 kcal·mol^{-1} from that of M06-2X and ωB97X-D functionals. In addition, the positive ΔE of the pre-reactant complex obtained at B3LYP functional predicts that no PRC being formed in the entrance channel of rn1 and rn5 reactions. However, the negative ΔE values as predicted by the M06-2X and ωB97X-D levels indicates a stabilized PRCs that accounts for the inaccuracy of B3LYP in predicting the

PRC states. This might be due to the lack of dispersion corrections in B3LYP, that may lead to the underestimation of intermolecular interactions stabilizing the reactant complexes (Park et al., 2019).

The computed activation barrier energies (**Table 1**) of the H-abstraction from HCHO (rn1) are found to be 9.09, 9.07 and 9.22 kcal·mol^{-1} at M06-2X/6-311+G(d,p), M06-2X/6-311++G(d,p), M06-2X/6-311++G(2d,2p) levels of theory. These values are slightly higher than the experimental value 7.90 kcal·mol^{-1} (Kerr & Parsonage, 1976), indicating a modest overestimation. Whereas the activation barrier energies obtained using B3LYP/6-311+G(d,p), B3LYP/6-311++G(d,p), B3LYP/6-311++G(2d,2p) levels are (5.54, 5.56 and 5.76 kcal·mol^{-1}) and ωB97X-D/6-311+G(d,p), ωB97X-D/6-311++G(d,p), ωB97X-D/6-311++G(2d,2p) levels ~6 kcal·mol^{-1} significantly underestimates the experimental value by approximately 2-3 kcal·mol^{-1}. As can be seen from **Table 1**, the activation barrier of 11.97 kcal·mol^{-1} for FCHO (rn2) and 12.30 kcal·mol^{-1} for CH_3CHO (rn5) calculated at M06-2X/6-311++G(d,p) level of theory agrees well with the previously reported experimental and theoretical [CCSD(T) and QCISD(T) levels] results. In contrast, the activation barriers calculated using B3LYP and ωB97X-D functionals for the reactions rn2 and rn5 are found to be underestimated by the amount of ~4.2 and ~3.2 kcal·mol^{-1} with that of the available results. Such an agreeable prediction of activation energy by M06-2X level with its high HF exchange (54%) and meta GGA correlation shows its effectiveness in the better prediction of barrier heights through improved electron density localization in the transition state (Mahmood and Longo, 2016).

Among the series of substituents studied, the H-abstraction mechanism exhibits notably higher activation energies for FCHO (TS2) and CH_3CHO (TS5) across all computational levels. Such higher activation energies observed for these substituents might be due to the stronger C-H bond dissociation and lack of stabilizing interactions in the corresponding transition state (Mora-Diez et al., 2001). This higher activation energy is structurally supported by the product-like geometry of TS2 (**Figure 3**), which may further lead to delayed TS along the reaction coordinate. In contrast, the most favourable abstraction channel with lower activation energy is observed for rn3 (ClCHO) (8.12 kcal·mol^{-1}) computed at M06-2X/6-311++G(d,p) level of theory indicates enhanced reactivity towards methyl radical. Though B3LYP and ωB97X-D predict the same reactivity ordering, they always underestimate the activation barriers (**Table 1**). In the presence of implicit solvent (water) (**Table S6**), the formation of the PRCs computed at the B3LYP level shows positive interaction energies, indicating that the complexes are destabilized relative to the isolated reactants. In contrast, the M06-2X and ωB97X-D functionals, which incorporate long-range dispersion corrections, predict the formation of PRCs (rn2–rn7) with slightly less negative ΔEs than the gas phase. Such a reduction in ΔEs reflects weak non-bonded interactions that are present between the reactants in their PRC state, which might be due to the competitive solvation effects around the solutes (Varghese and Mushrif, 2019).

3.3 Feasibility and Spontaneity of the Reactions

In order to understand the feasibility and spontaneity of the reactions (rn1-rn7), the reaction enthalpy ($\Delta H_{(rxn)}$,overall heat change of the reaction from reactants to products), change in internal energy ($\Delta \mathbf{E}^{\ddagger}_{\mathbf{0}\boldsymbol{K}}$, sum of electronic and zero-point energies), change in Gibb's free energy ($\Delta \mathbf{G}^{\ddagger}_{\mathbf{298}\,\boldsymbol{K}}$) and change in activation enthalpy ($\Delta \mathbf{H}^{\ddagger}_{\mathbf{298}\,\boldsymbol{K}}$), relative to reactants are listed in **Table 1** (Dodd, 1955; Su and Francisco, 1995; Kerr and Parsonage, 1976; Liu et al., 2003; Ruscic et al., 2004; Ruscic et al., 2005; Zokaie et al., 2021) and 2 for both gas and water phases. The considered reactions are found to be exothermic in nature with negative enthalpy change. However, the H-abstraction reaction involving fluorinated aldehyde (FCHO) shows a significantly lesser negative enthalpy change with that of other substituents, suggesting the reaction to be weakly exothermic (Mora-Diez et al., 2001).

Table 1. Change in internal energies $\Delta E^{\ddagger}_{0K}$, enthalpies $\Delta H^{\ddagger}_{298K}$, Gibbs free energies $\Delta G^{\ddagger}_{298K}$and reaction enthalpy (ΔH (rxn)) (kcal.mol^{-1}) of the seven H-abstraction reactions (rn1-rn7) calculated at all nine levels of theory in gas phase.

Reactions	$\Delta E^{\ddagger}_{0K}$ (sum of electronic and zero point energies)							$\Delta H^{\ddagger}_{298K}$						
Level of theory	**rn1**	**rn2**	**rn3**	**rn4**	**rn5**	**rn6**	**rn7**	**rn1**	**rn2**	**rn3**	**rn4**	**rn5**	**rn6**	**rn7**
B3LYP/6-311+G(d,p)	5.547	9.097	4.755	5.693	8.998	6.299	6.279	4.741	8.220	3.84	5.021	8.216	5.573	5.611
B3LYP/6-311++G(d,p)	5.564	9.087	4.789	5.638	9.148	6.333	6.254	4.740	8.197	3.818	5.023	8.200	5.555	5.539
B3LYP/6-311++G(2d,2p)	5.760	9.323	4.970	5.862	9.428	6.537	6.376	4.954	8.410	4.073	5.262	8.490	5.795	5.902
M06-2X/6-311+G(d,p)	9.091	11.98	8.129	9.212	12.16	9.819	9.201	8.010	11.00	7.213	8.305	11.04	9.118	8.558
M06-2X/6-311++G(d,p)	9.069	11.97	8.122	9.184	12.30	10.06	9.613	7.988	10.99	7.201	8.328	11.09	9.226	8.758
M06-2X/6-311++G(2d,2p)	9.222	11.80	8.121	9.376	12.54	9.390	9.128	8.018	10.86	7.200	8.381	11.22	9.003	8.501
ωB97XD/6-311+G(d,p)	5.980	9.211	5.173	5.828	9.032	6.414	6.394	4.982	8.240	4.321	4.976	7.834	5.578	5.506
ωB97XD/6-311++G(d,p)	5.961	9.241	5.173	5.926	9.420	6.784	6.557	4.963	8.229	4.34	5.008	7.942	5.692	5.568
ωB97XD/6-311++G(2d,2p)	6.152	9.341	5.299	6.106	9.678	6.960	6.842	5.150	8.362	4.519	5.225	8.208	5.906	5.823
Literature values	10.7[c]	13.5[a]		8.74[b]	12.60[b]			7.90[f]*			8.3[d]*	10.0*		

Reactions	$\Delta G^{\ddagger}_{298K}$							$\Delta H_{(rxn)}$						
Level of theory	**rn1**	**rn2**	**rn3**	**rn4**	**rn5**	**rn6**	**rn7**	**rn1**	**rn2**	**rn3**	**rn4**	**rn5**	**rn6**	**rn7**
B3LYP/6-311+G(d,p)	11.506	16.473	12.006	13.347	17.218	13.271	13.759	-17.009	-3.776	-13.461	-16.279	-11.165	-12.973	-12.614
B3LYP/6-311++G(d,p)	12.347	16.460	12.046	12.821	17.192	13.466	13.464	-17.002	-3.761	-13.414	-16.261	-11.173	-12.942	-12.572
B3LYP/6-311++G(2d,2p)	12.303	16.936	11.247	13.038	17.438	13.180	13.739	-17.075	-3.757	-13.687	-16.269	-11.178	-12.986	-14.187
M06-2X/6-311+G(d,p)	15.651	19.326	14.865	15.997	19.060	16.496	15.837	-16.176	-2.667	-12.403	-15.305	-9.679	-11.702	-10.852
M06-2X/6-311++G(d,p)	15.611	19.286	14.829	14.815	18.922	16.165	15.240	-16.175	-2.664	-12.362	-15.299	-9.690	-11.681	-10.867
M06-2X/6-311++G(2d,2p)	15.663	19.215	14.935	15.026	18.957	15.562	14.406	-16.533	-2.834	-12.947	-15.574	-9.874	-12.031	-12.703
ωB97XD/6-311+G(d,p)	13.211	16.005	12.190	13.197	17.069	13.684	13.158	-17.253	-3.919	-13.439	-16.337	-10.533	-13.004	-12.192
ωB97XD/6-311++G(d,p)	13.198	16.491	11.638	12.462	16.746	13.435	13.083	-17.249	-3.908	-13.448	-16.325	-10.538	-12.975	-12.156
ωB97XD/6-311++G(2d,2p)	13.478	16.849	12.026	12.220	17.096	13.822	13.482	-17.192	-3.806	-13.550	-16.215	-10.483	-12.918	-12.270
Expt*								-14.71* -16.74[c]	-0.7*		-15.73[e]	-9.25[e]		

[a]QCISD(T)/6-311++G(2df,2p),(Su & Francisco, 1995) [b]CCSD(T,full)/aug-cc-pVTZ+2df//CCD/6–311+G(2d,2p) (Zokaie et al., 2021) [c]QCISD(T)/6-311+G(3df,2p) (Liu et al., 2003) *-Experimental: [d](300-564 K), (Dodd, 1955), [e](Ruscic et al., 2004; Ruscic et al., 2005) [f](Kerr and Parsonage, 1976).

Table 2. Change in internal energies $\Delta E^{\ddagger}_{0K}$, enthalpies $\Delta H^{\ddagger}_{298K}$, Gibbs free energies $\Delta G^{\ddagger}_{298K}$and reaction enthalpy (ΔH (rxn)) (kcal.mol^{-1}) of the seven H-abstraction reactions (rn1-rn7) calculated at all nine levels of theory in water phase.

Reactions	$\Delta E^{\ddagger}_{0K}$							$\Delta H^{\ddagger}_{298K}$						
Level of theory	**rn1**	**rn2**	**rn3**	**rn4**	**rn5**	**rn6**	**rn7**	**rn1**	**rn2**	**rn3**	**rn4**	**rn5**	**rn6**	**rn7**
B3LYP/6-311+G(d,p)	6.783	10.113	5.314	6.716	8.951	7.454	7.112	5.943	9.448	4.740	6.089	7.990	6.891	6.593
B3LYP/6-311++G(d,p)	6.780	10.048	5.286	6.702	8.928	7.386	7.063	5.940	9.421	4.711	6.082	7.977	6.870	6.544
B3LYP/6-311++G(2d,2p)	6.951	10.203	5.515	6.893	9.179	7.580	7.357	6.136	9.572	4.946	6.301	8.234	7.061	6.856
M06-2X/6-311+G(d,p)	9.495	12.732	9.074	9.278	11.753	10.922	10.289	8.486	11.836	7.779	8.234	10.612	9.997	9.388
M06-2X/6-311++G(d,p)	9.481	12.721	8.291	9.251	11.835	10.924	10.271	8.472	11.800	7.180	8.195	10.657	10.004	9.377
M06-2X/6-311++G(2d,2p)	9.444	12.538	8.276	9.248	11.869	10.926	10.270	8.421	11.632	7.171	8.205	10.685	9.999	9.409
ωB97XD/6-311+G(d,p)	6.857	10.131	5.566	6.639	8.874	7.398	7.047	5.904	9.212	4.672	5.601	7.458	6.317	6.056
ωB97XD/6-311++G(d,p)	6.854	10.061	5.589	6.669	9.030	7.339	7.095	5.899	9.183	4.648	5.604	7.532	6.308	6.035
ωB97XD/6-311++G(2d,2p)	7.124	10.115	5.690	6.823	8.793	7.521	7.309	6.147	9.341	4.856	5.897	7.796	6.472	6.263

Reactions	$\Delta G^{\ddagger}_{298K}$							$\Delta H_{(rxn)}$						
Level of theory	**rn1**	**rn2**	**rn3**	**rn4**	**rn5**	**rn6**	**rn7**	**rn1**	**rn2**	**rn3**	**rn4**	**rn5**	**rn6**	**rn7**
B3LYP/6-311+G(d,p)	14.007	17.839	12.211	14.259	17.041	15.462	15.100	-15.246	-0.939	-10.888	-14.775	-10.720	-10.424	-10.571
B3LYP/6-311++G(d,p)	13.980	17.167	12.273	14.139	16.918	14.586	15.039	-15.248	-0.924	-10.849	-14.772	-10.724	-10.400	-10.535
B3LYP/6-311++G(2d,2p)	13.855	17.277	12.420	13.807	17.153	14.954	15.216	-15.326	-1.021	-11.221	-14.800	-10.759	-10.513	-10.831
M06-2X/6-311+G(d,p)	17.455	20.648	15.993	15.863	18.026	17.609	15.862	-14.437	0.182	-9.749	-13.786	-9.706	-9.281	-9.013
M06-2X/6-311++G(d,p)	17.443	20.616	15.951	15.968	18.612	17.526	15.698	-14.443	0.186	-9.714	-13.790	-9.709	-9.266	-8.988
M06-2X/6-311++G(2d,2p)	17.443	20.462	16.007	16.106	18.565	17.420	15.164	-14.794	-0.068	-10.395	-14.076	-9.653	-9.428	-9.320
ωB97XD/6-311+G(d,p)	14.655	18.022	13.003	13.233	16.191	14.455	14.398	-15.471	-1.045	-10.817	-14.787	-10.351	-10.639	-10.310
ωB97XD/6-311++G(d,p)	14.656	17.799	19.675	13.326	16.994	14.450	14.317	-15.476	-1.033	-10.826	-14.789	-10.351	-10.617	-10.279
ωB97XD/6-311++G(2d,2p)	15.022	18.247	13.308	13.754	17.048	14.663	14.613	-15.412	-1.027	-11.016	-14.878	-10.302	-10.597	-10.439

According to the data from the NIST-JANAF thermochemical tables (Chase, 1998) and the Active Thermochemical Tables (ATcT), (Ruscic et al., 2004; Ruscic et al., 2005) the reaction enthalpies of the reactions (rn1, rn2 and rn4) involving HCHO, FCHO and CH_3CHO by methyl radical at 298 K are found to be -14.63, -0.7, -15.45 and -9.25 kcal·mol^{-1} respectively. By comparing the reaction enthalpies among the levels used, the best estimated value is found to be -16.17, -2.66, -15.23 and -9.3 kcal·mol^{-1} for rn1, rn2, rn4 and rn5 reactions computed at M06-2X/6-311++G(d,p) level of theory.

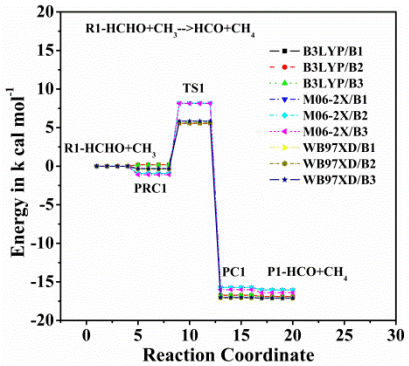

(a) rn1

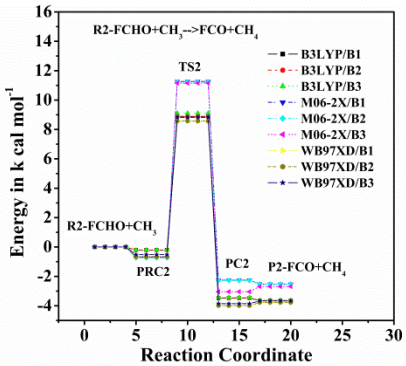

(b) rn2

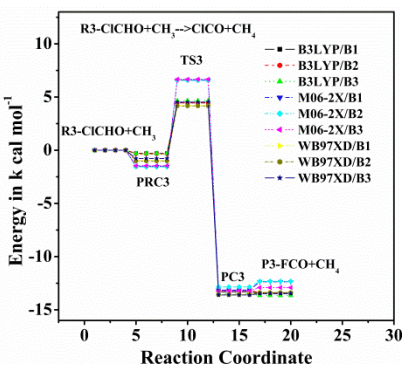

(c) rn3

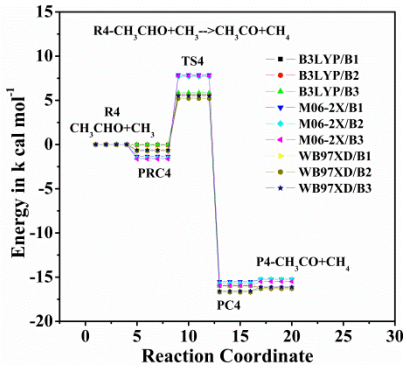

(d) rn4

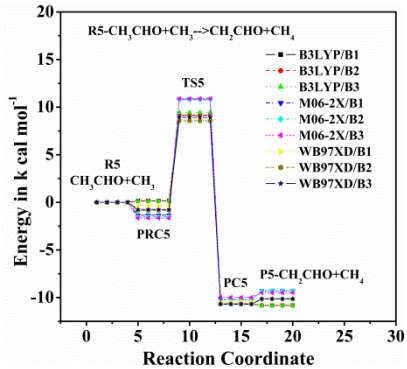

(e) rn5

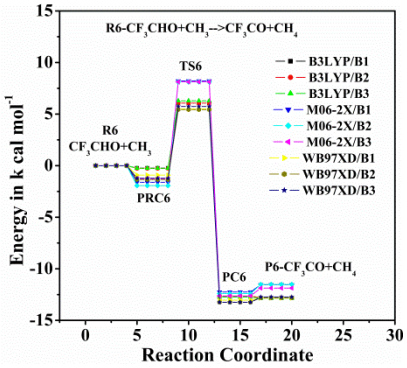

(f) rn6

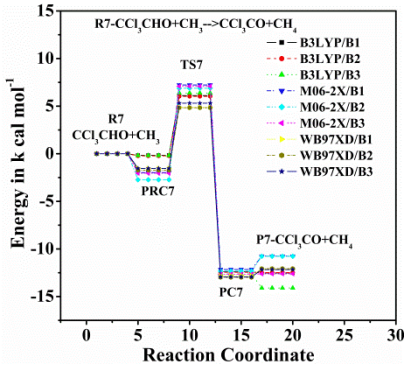

(g) rn7

(1)

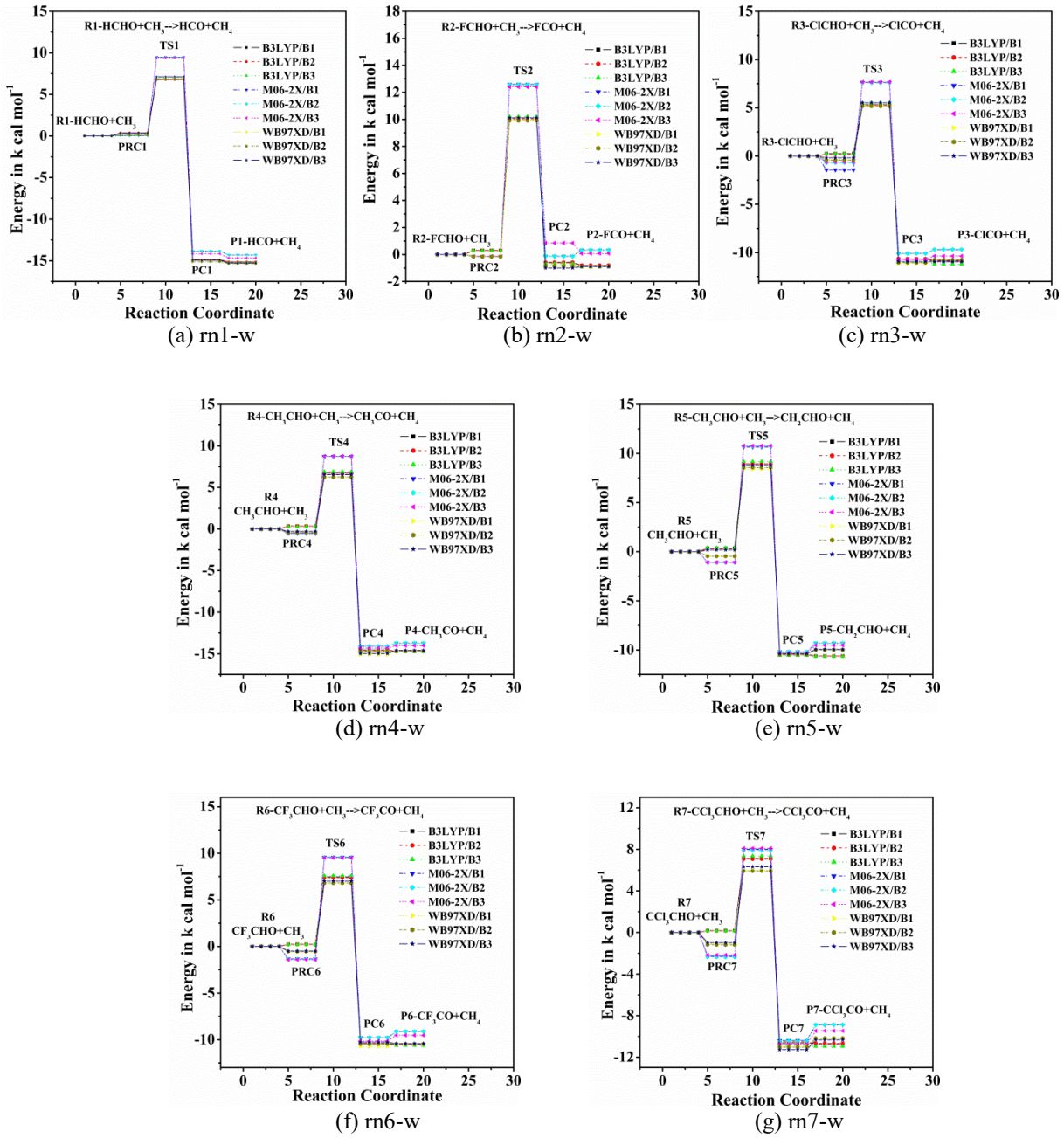

(a) rn1-w (b) rn2-w (c) rn3-w

(d) rn4-w (e) rn5-w

(f) rn6-w (g) rn7-w

(2)

Figure 4. (1) (a-g) Relative energy profiles for the H- abstraction reactions from aldehydes by $\dot{C}H_3$radical in gas phase calculated using B3LYP, M06-2X and ωB97XD in conjunction with (B1) 6-311+G(d,p), (B2) 6-311++G(d,p) and (B3) 6-311++G(2d,2p) level of theory for (a) rn1 (Formaldehyde) (b) rn2 (Formyl fluoride) (c) rn3 (Formyl chloride) (d-e) rn4 & rn5 (Acetaldehyde) (f) rn6 (Trifluoroacetaldehyde) and (g) rn7 (Trichloroacetaldehyde). **(2)** (a-g) Relative energy profiles for the H- abstraction reactions from aldehydes by $\dot{C}H_3$ radical in water phase calculated using B3LYP, M06-2X and ωB97XD in conjunction with (B1) 6-311+G(d,p), (B2) 6-311++G(d,p) and (B3) 6-311++G(2d,2p) level of theory for (a) rn1-w (Formaldehyde) (b) rn2-w (Formyl fluoride) (c) rn3-w (Formyl chloride) (d-e) rn4-w & rn5-w (Acetaldehyde) (f) rn6-w Trifluoroacetaldehyde) and (g) rn7-w (Trichloroacetaldehyde).

From **Tables 1** and **2**, as the activation barrier of ClCHO reaction (rn3) is comparable to HCHO (rn1), we infer that chlorine substitution does not significantly affect the energetics of H- abstraction process. However, the F substituted aldehyde (FCHO) (rn4) markedly increases the activation barrier energy by the order of about 3 kcal·mol^{-1}. This is in conjunction with the reported results of H-abstraction process from halogenated aldehydes by ȮH (Francisco, 1992). Overall analyses on the thermodynamic data (**Tables 1** and **2**) suggests that H- abstraction is highly feasible for reactions rn1 and rn4 with significant negative reaction enthalpies (ΔH_{rxn}). A slightly reduced thermodynamic feasibility with moderate negative (ΔH_{rxn}) values is observed for rn3, rn5, rn6 and rn7. However, reaction rn2 involving FCHO exhibits the least feasibility with significantly lesser negative (ΔH_{rxn}) values in both gas and water phases.

3.4 Temperature Dependence of Rate Constant

The rate constants of H-abstraction pathways (rn1-rn7) were calculated using conventional transition state theory (TST) over the temperature range of 300-1700 K. **Figures 5(1) a**nd **5(2)** show the temperature dependent rate constants of rn1-rn7 reactions to analyse the predicted kinetics across different levels of theory. It can be seen from **Figures 5(1)** & **5(2)** that the reactions exhibit non-Arrhenius behaviour with respect to temperatures, further attributing to positive temperature dependence (Laidler, 1969). Referring **Tables S7-S13** and **Figures 5(1)a-5(1)g**, it can be understood that H- abstraction reactions of rn1, rn3, rn4 and rn7 at 300 K exhibit the rate constant (k_{Eck}) in the order of 10^{-17} cm^3 molecule^{-1} s^{-1}, in contrast to reactions rn2, rn5 and rn6 where the rate constant decreases to 10^{-21} cm^3 molecule^{-1} s^{-1}. These observations correlate with the higher activation energies associated with the corresponding reaction pathways rn2, rn5 and rn6 as shown in **Figures 4(1, a-g).**

Figures 5(1)a, **5(1)d**, and **5(1)e** (Dodd, 1951; Volman and Brinton, 1952; Dodd, 1955; Kerr and Calvert, 1965; Liu and Laidler, 1968; Kerr and Parsonage, 1976; Manthorne and Pacey, 1978; Anastasi, 1983; Choudhury et al., 1989; Liu et al., 2003; Yasunaga et al., 2008; Mendes et al., 2014; Nguyen and Nguyen, 2018; Zokaie et al., 2021) presents comparative plots of the calculated rate constants for reaction channels rn1, rn4, and rn5. These results are benchmarked against available experimental and previously reported theoretical values, enabling a comprehensive assessment of methodological consistency and predictive accuracy. For channel rn1 (**Figure 5(1)a** and **Table S7**), the computed rate constant at 300 K of the order of 9.65x10^{-18}, 1.03x10^{-17} and 1.14x10^{-17} cm^3 molecule^{-1} s^{-1} using M06-2X functional with basis sets 6-311+G(d,p), 6-311++G(d,p) and 6-311++G(2d,2p) shows good agreement with experimental data. In contrast, with the computed rate constants of rn1 reaction of about 6.83x10^{-16} and 5.37x10^{-16} cm^3 molecule^{-1} s^{-1}, the B3LYP functional with basis sets (6-311++G(d,p) and 6-311++G(2d,2p)) significantly overestimates the experimental values. At high temperatures (1300-1700 K), both M06-2X and ωB97XD functionals yields rate constant that closely match the experimental results as reported by Choudhury et al (Choudhury et al., 1989). For channel rn4, the rate computed at M06-2X/6-311++G(2d,2p) agrees well with experimental data in the 400-1000 K range, with an error factor less than 2. At elevated temperatures (1500-1700 K), both M06-2X/6-311+G(d,p) and ωB97XD/6-311+G(d,p) are in good consistency with experimental results. The observed rate constant of aldehydes and halogenated aldehydes by methyl radical is about 3-5 orders of magnitude smaller in comparison with OH radical (Chandra, Uchimaru, & Sugie, 2001; Wallington & Hurley, 1993) and the observed rate for the reactions rn2 and rn3 is almost comparable to the rate obtained by FCHO and ClCHO with NO_3 radical (Mora-Diez & Boyd, 2002) at 298 K (refer **Tables S8** and **S9**). These results imply that the reactivity of $\dot{C}H_3$ can compete with NO_3 radical highlighting the importance of title reaction.

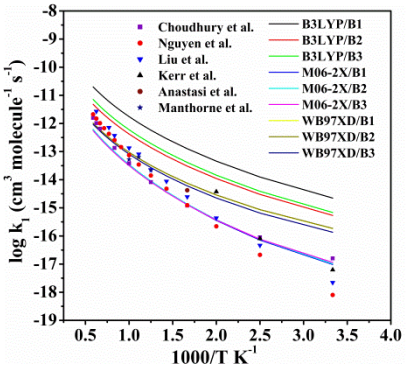

(a) k1

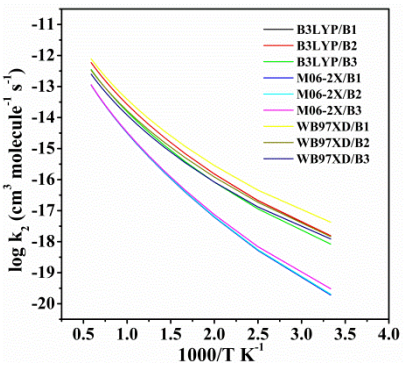

(b) k2

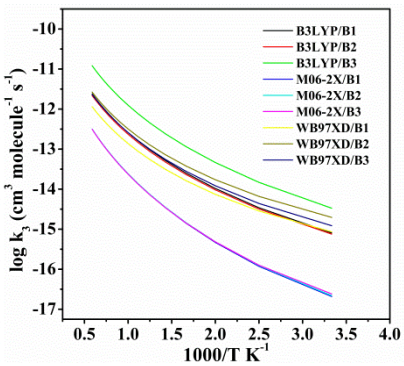

(c) k3

*References cited in Figure (a) k1: (Kerr and Parsonage, 1976; Manthorne and Pacey, 1978; Anastasi, 1983; Choudhury et al., 1989; Liu et al., 2003; Nguyen and Nguyen, 2018).

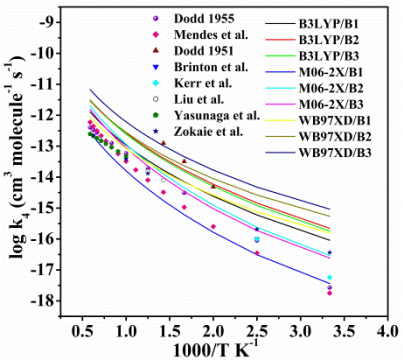

(d) k4

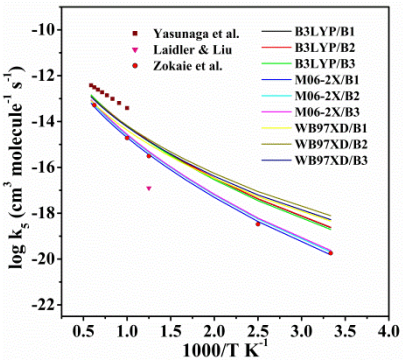

(e) k5

*References cited in Figure (d & e) k4 and k5: (Dodd, 1951; Volman and Brinton, 1952; Dodd, 1955; Kerr and Calvert, 1965; Liu and Laidler, 1968; Yasunaga et al., 2008; Mendes et al., 2014; Zokaie et al., 2021).

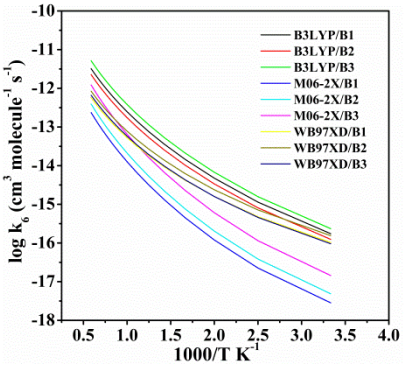

(f) k6

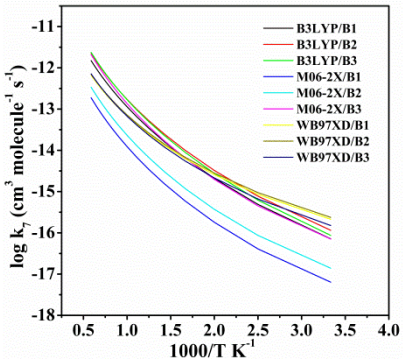

(g) k7

(1)

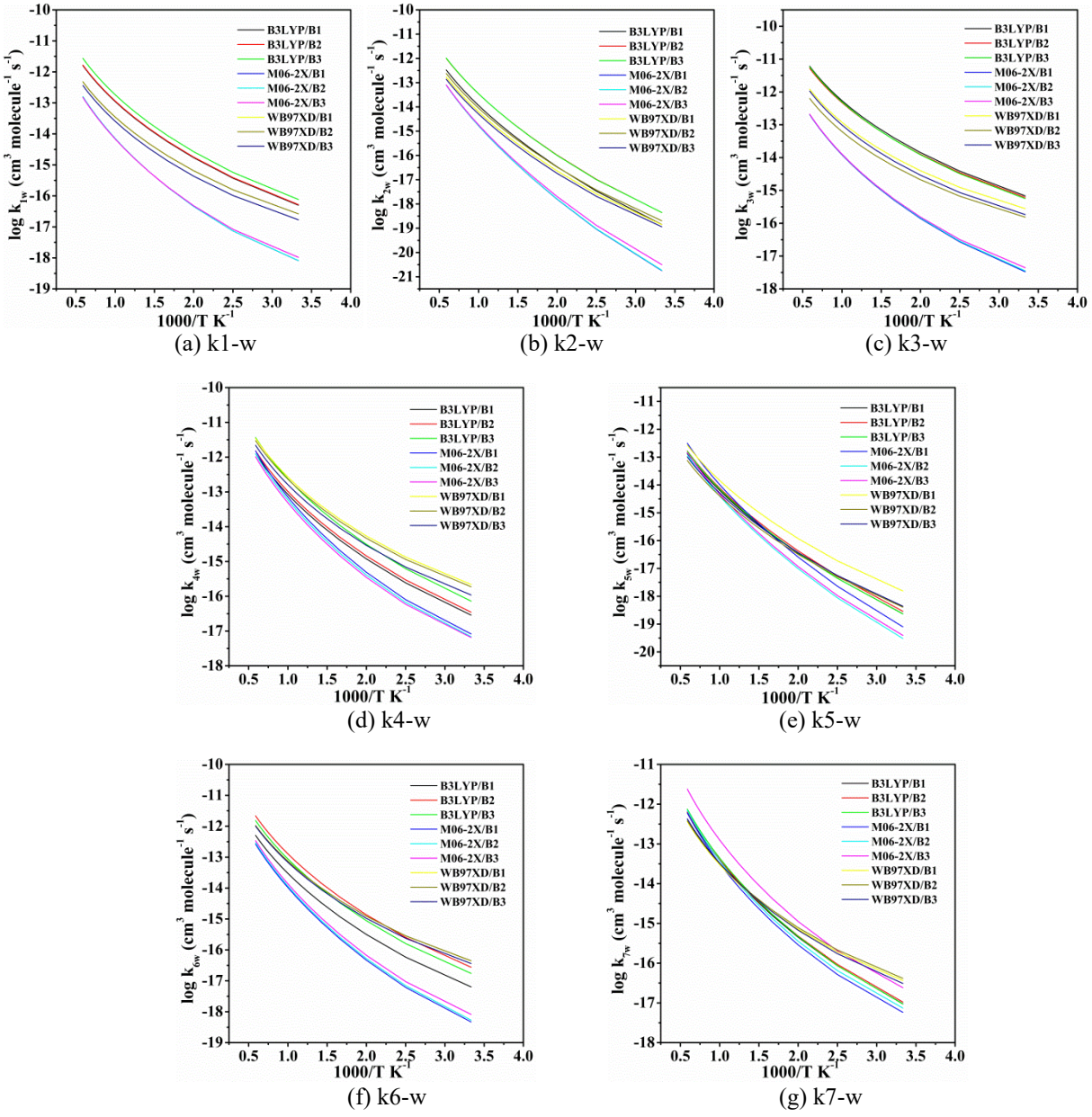

(a) k1-w (b) k2-w (c) k3-w

(d) k4-w (e) k5-w

(f) k6-w (g) k7-w

(2)

Figure 5. (1) (a-g) Rate constants (k1-k7) for the hydrogen abstraction reaction (rn1-rn7) over the temperature range of 300-1700 K calculated by TST/Eck, compared available literature values in gas phase. **(2)** (a-g) Rate constants (k1-k7) for the hydrogen abstraction reaction (rn1-rn7) over the temperature range of 300-1700 K calculated by TST/Eck, in water phase.

To account for quantum mechanical effects, tunnelling corrections were incorporated using Eckart tunnelling model and **Figure 6**. illustrates the variation of tunnelling transmission coefficient [X(T)] as a function of temperature (K). The quantum tunnelling effects are found to be significant at low temperatures (300-400 K) with the higher transmission coefficients of the order of ~38.8 that further

supports the non-Arrhenius (Laidler, 1969) behaviour of the reaction kinetics observed in **Figures 5(1)** and **5(2)**. At elevated temperatures (1100-1700 K), tunnelling becomes negligible with the coefficients typically approaching to unity (~1.2) inducing the reaction to proceed within the classical limit (Truong & Duncan, 1999).

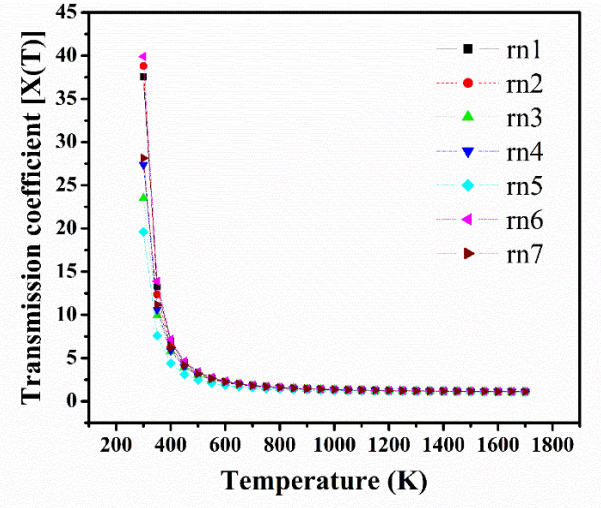

Figure 6. Variation of tunnelling transmission coefficient [X(T)] as a function of temperature (K) for the reactions rn1-rn7.

This behaviour highlights the temperature sensitivity of these reactions, wherein hydrogen atom tunnel through the activation energy barrier, allowing the reaction to proceed at low temperatures where classical activation is improbable. Though water-assisted reactions exhibit reduced rate constants (**Tables S14-S20**), they follow the same mechanism as that of the gas phase reactions.

4. Conclusions

This study assessed the performance of three DFT functionals B3LYP, M06-2X and ωB97XD paired with basis sets 6-311+G(d,p), 6-311++G(d,p) and 6-311++G(2d,2p) in modelling the non-catalytic H-abstraction reactions of aldehydes (XCHO, where X=CH_3, CF_3, CCl_3, H, F, Cl) in the presence of methyl radical in both gas and water phases. The stabilization of the PRC, observed at the M06-2X and ωB97X-D levels is found to be absent in B3LYP method, which emphasizes the importance of dispersion interactions in accurately determining the PRCs. The most favourable H- abstraction pathways with characteristic activation energies occur for ClCHO (rn3) and CH_3CHO (rn4) reactions. A significant alteration in the activation barrier of Fluorine substituted aldehyde is primarily due to the reduced stabilization of its transition state and product radical. The results revealed that the M06-2X functional yielded more accurate activation barriers, reaction enthalpies and rate constants with Eckart tunnelling correction when compared with the available experimental and high-level theoretical data. The ωB97X-D/6-311++G(2d,2p) shows reasonable accuracy for activation barriers and rate constant especially at elevated temperatures (1300-1700 K). Whereas, B3LYP underestimate barrier energies and overestimate rate constants indicating its reduced reliability for temperature dependent reaction kinetics.

However, the rate calculation based on reaction energetics support the reactivity trend as: rn4>rn3>rn7>rn1>rn6>rn5>rn2 at all the considered levels of theory. The studied reactions exhibit

temperature-dependent kinetics with non-Arrhenius behaviour arising from quantum tunnelling at low temperatures and classical thermal activation prevailing at higher temperatures. Overall, this benchmarking approach identifies M06-2X functional as the most thermodynamically consistent and accurate method for modelling H-abstraction reaction kinetics of aldehydes and halogenated aldehydes, with ωB97X-D functional offering a slightly comparable reliability.

Appendix

Supplementary Information

Non-Catalytic Hydrogen Abstraction Kinetics of Aldehyde–Methyl Radical Reactions: A DFT Benchmark Perspective

Table S1-S2. Geometric parameters of the reactant and product species involved in the H-abstraction reactions in gas phase computed at all nine levels of theory.

Table S3-S4. Key Geometric parameters of the Transition state structures for H- abstraction reaction from substituted aldehydes XCHO (X = H, F, Cl, CH_3, CF_3, CCl_3) by Methyl radical ($\dot{C}H_3$) in gas and water phase computed at all nine levels of theory.

Table S5-S6. Relative energy profiles (ΔE)(kcal.mol^{-1}) for the H- abstraction reactions (rn1-rn7) of aldehydes and halogenated aldehydes with $\dot{C}H_3$radical calculated at all nine levels of theory in gas and water phase.

Table S7-S13. Rate constant (cm^3 molecule^{-1} s^{-1}) for the reactions (rn1-rn7) $CH_3CHO + \dot{C}H_3 \rightarrow CH_3\dot{C}O + CH_4$ in the temperature range 300-1700 K, at 1 atm pressure in gas phase.

Table S14-S20. Rate constant (cm^3 molecule^{-1} s^{-1}) for the reactions (rn1-rn7) $CH_3CHO + \dot{C}H_3 \rightarrow CH_3\dot{C}O + CH_4$ in the temperature range 300-1700 K, at 1 atm pressure in water phase.

Table S1. Geometric parameters of the reactant species involved in the H- abstraction reaction in gas phase computed at all nine levels of theory.

Level of theory	Geometrical parameters (Å) / (°)																							
	HCHO			FCHO				ClCHO				CH_3CHO				CF_3CHO				CCl_3CHO			
	C1-O2	C1-H3	H3-C1-O2	C1-O2	C1-H3	C1-F4	H3-C1-O2	C1-O2	C1-H3	C1-Cl4	H3-C1-O2	C2-O3	C2-H7	C1-C2	C1-C2-H7	C2-O3	C2-H4	C1-C2	C1-C2-H4	C2-O3	C2-H4	C1-C2	C1-C2-H4
B3LYP/6-311+G(d,p)	1.202	1.108	122	1.177	1.095	1.355	128.4	1.179	1.096	1.796	127	1.206	1.112	1.504	115.1	1.194	1.106	1.547	113.1	1.192	1.105	1.551	111.7
B3LYP/6-311++G(d,p)	1.202	1.108	122	1.177	1.095	1.355	128.4	1.179	1.096	1.796	127.1	1.206	1.112	1.504	115.1	1.194	1.106	1.547	113.1	1.192	1.105	1.551	111.7
B3LYP/6-311++G(2d,2p)	1.201	1.105	121.8	1.176	1.093	1.353	128.2	1.177	1.093	1.796	126.9	1.205	1.109	1.502	115.3	1.193	1.103	1.544	113.1	1.191	1.102	1.547	111.9
M06-2X/6-311+G(d,p)	1.197	1.105	121.7	1.173	1.095	1.338	127.9	1.175	1.096	1.773	126.8	1.209	1.102	1.502	115.6	1.188	1.104	1.539	113.6	1.186	1.104	1.546	111.9
M06-2X/6-311++G(d,p)	1.197	1.105	121.7	1.173	1.095	1.338	127.9	1.175	1.096	1.773	126.8	1.209	1.102	1.502	115.6	1.188	1.104	1.539	113.6	1.186	1.104	1.546	111.8
M06-2X/6-311++G(2d,2p)	1.196	1.103	121.6	1.173	1.093	1.337	127.7	1.174	1.093	1.774	126.6	1.207	1.107	1.505	115.7	1.188	1.102	1.536	113.8	1.185	1.102	1.541	112.2
ωB97XD/6-311+G(d,p)	1.198	1.107	121.9	1.174	1.095	1.343	128.1	1.176	1.097	1.778	126.7	1.202	1.111	1.501	115.3	1.190	1.105	1.544	113.3	1.187	1.105	1.549	111.9
ωB97XD/6-311++G(d,p)	1.198	1.107	121.9	1.174	1.095	1.343	128.1	1.176	1.097	1.778	126.7	1.202	1.111	1.501	115.3	1.19	1.105	1.544	113.3	1.187	1.105	1.549	111.9
ωB97XD/6-311++G(2d,2p)	1.197	1.105	121.7	1.174	1.094	1.34	127.9	1.175	1.099	1.777	126.6	1.201	1.499	1.499	115.4	1.189	1.103	1.542	113.5	1.187	1.103	1.546	112.1
***Literature (Francisco, 1992; Berney, 1969; Chandra et al., 2001)**	1.2	1.105	121.8	1.181	1.095	1.338	127.3	1.175	1.094	1.798	126.7	1.216	1.114	1.501	117.5	1.204	1.09	1.54	120.0	1.199	1.105	1.545	111.6

Table S2. Geometric parameters of the product species involved in the H- abstraction reaction in gas phase computed at all nine levels of theory.

Level of theory	Geometrical parameters (Å) / (°)																							
	HCO			FCO			ClCO			CH_3CO			CH_2CHO			CF_3CO			CCl_3CO			CH_4		CH_3	
	C2-H3	H3-C2-O1	C2-O1	F1-C2	F1-C2-O3	C2-O3	Cl1-C2	C2-O3	Cl1-C2-O3	C2-O1	C2-C3	O1-C2-C3	C2-C4	C2-H3	H1-C2-H3	C1-C4	C1-O2	O2-C1-C4	C4-C5	C5-O6	C4-C5-O6	C-H	H-C-H	C-H	H-C-H
B3LYP/6-311+G(d,p)	1.125	124.574	1.174	1.337	127.567	1.167	1.832	1.155	120.990	1.180	1.509	129.009	1.424	1.084	119.595	1.568	1.169	125.545	1.545	1.169	129.595	1.091	109.595	1.081	120.000
B3LYP/6-311++G(d,p)	1.125	124.574	1.174	1.337	127.567	1.167	1.832	1.155	120.990	1.180	1.509	129.009	1.424	1.084	119.595	1.568	1.169	125.545	1.545	1.169	129.595	1.091	109.595	1.081	120.000
B3LYP/6-311++G(2d,2p)	1.122	124.273	1.173	1.336	127.567	1.166	1.832	1.153	120.994	1.179	1.508	128.808	1.420	1.081	119.596	1.566	1.168	125.542	1.542	1.167	129.596	1.088	109.596	1.078	120.000
M06-2X/6-311+G(d,p)	1.122	124.373	1.168	1.323	127.568	1.161	1.817	1.149	120.992	1.173	1.512	128.408	1.430	1.082	119.597	1.566	1.163	125.544	1.558	1.179	129.597	1.089	109.597	1.079	120.000
M06-2X/6-311++G(d,p)	1.122	124.373	1.168	1.323	127.568	1.161	1.817	1.149	120.992	1.173	1.512	128.408	1.430	1.082	119.597	1.566	1.163	125.544	1.555	1.178	129.597	1.089	109.597	1.079	120.000
M06-2X/6-311++G(2d,2p)	1.120	123.972	1.167	1.322	127.568	1.160	1.823	1.147	120.994	1.172	1.511	128.208	1.426	1.079	119.598	1.564	1.162	125.542	1.544	1.178	129.598	1.087	109.598	1.076	120.000
ωB97XD/6-311+G(d,p)	1.123	124.574	1.171	1.333	127.567	1.164	1.801	1.154	120.990	1.176	1.508	129.009	1.424	1.084	119.595	1.567	1.166	125.545	1.551	1.178	129.595	1.091	109.595	1.081	120.000
ωB97XD/6-311++G(d,p)	1.123	124.574	1.171	1.333	127.567	1.164	1.801	1.154	120.990	1.176	1.508	129.009	1.424	1.084	119.595	1.567	1.166	125.545	1.551	1.178	129.595	1.091	109.595	1.081	120.000
ωB97XD/6-311++G(2d,2p)	1.121	124.273	1.170	1.332	127.567	1.163	1.801	1.152	120.994	1.175	1.507	128.808	1.420	1.081	119.596	1.565	1.165	125.542	1.542	1.177	129.596	1.088	109.596	1.078	120.000
Literature*	1.125	125.0	1.175	1.334	127.3	1.169	1.800	1.163	120.988	1.187	1.520	127.5	1.440	1.106	118.1	1.557	1.177	124.2	1.556	1.173	127.7	1.087	109.594	1.07	120.000

Table S3. Key Geometric parameters of the transition state structures for H- abstraction reaction from substituted aldehydes XCHO (X = H, F, Cl, CH_3, CF_3, CCl_3) by Methyl radical ($\dot{C}H_3$) in gas phase computed at all nine levels of theory.

Level of theory	Geometrical parameters(Å) / (°)																				
	TS1 (X=H)			TS2 (X=F)			TS3 (X=Cl)			TS4 (X=CH_3)			TS5 (X= CH_3)			TS6 (X=CF_3)			TS7 (X=CCl_3)		
	C1-H3	C4-H3	C1-H3-C4	C1-H3	C4-H3	C1-H3-C4	C1-H3	C4-H3	C1-H3-C4	C2-H7	C8-H7	C2-H7-C8	C1-H5	C8-H5	C1-H5-C8	C2-H4	C5-H4	C2-H4-C5	C2-H4	C5-H4	C2-H4-C5
B3LYP/6-311+G(d,p)	1.274	1.492	178	1.332	1.376	179.8	1.266	1.464	176.7	1.275	1.502	178.2	1.277	1.441	175.3	1.296	1.455	176.6	1.292	1.452	174
B3LYP/6-311++G(d,p)	1.274	1.493	178	1.332	1.376	179.8	1.267	1.464	176.8	1.275	1.502	178.3	1.277	1.442	175.3	1.296	1.455	176.6	1.291	1.456	174.6
B3LYP/6-311++G(2d,2p)	1.275	1.486	178.4	1.331	1.375	179.9	1.267	1.459	176.9	1.277	1.494	178.6	1.278	1.437	175.2	1.297	1.451	177	1.292	1.452	174.5
M06-2X/6-311+G(d,p)	1.266	1.482	174.8	1.322	1.372	179	1.264	1.449	179.3	1.265	1.495	178.6	1.27	1.433	175.8	1.287	1.448	179.5	1.285	1.447	179.1
M06-2X/6-311++G(d,p)	1.266	1.482	175	1.322	1.372	179	1.264	1.449	179.3	1.265	1.495	178.9	1.27	1.433	176.1	1.287	1.448	178.8	1.285	1.447	178.8
M06-2X/6-311++G(2d,2p)	1.266	1.477	175.3	1.32	1.373	178.9	1.264	1.444	178.8	1.265	1.489	179.4	1.27	1.43	176.1	1.287	1.445	179.2	1.285	1.444	179
ωB97XD/6-311+G(d,p)	1.272	1.475	179.6	1.333	1.358	179.4	1.274	1.435	179	1.27	1.487	178.9	1.28	1.416	176.4	1.294	1.435	178	1.294	1.431	177.5
ωB97XD/6-311++G(d,p)	1.272	1.476	176.7	1.333	1.358	179.6	1.274	1.435	178.6	1.27	1.487	179.3	1.28	1.416	176.5	1.295	1.434	178.4	1.293	1.432	178.1
ωB97XD/6-311++G(2d,2p)	1.273	1.47	177.1	1.333	1.357	179.5	1.274	1.431	178.6	1.271	1.48	179.6	1.281	1.412	176.3	1.295	1.432	179	1.294	1.429	178

Table S4. Key Geometric parameters of the transition state structures for H- abstraction reaction from substituted aldehydes XCHO (X = H, F, Cl, CH_3, CF_3, CCl_3) by Methyl radical ($\dot{C}H_3$) in solvent (water) phase computed at all nine levels of theory.

Level of theory	Geometrical parameters(Å) / (°)																				
	TS1 (X=H)			TS2 (X=F)			TS3 (X=Cl)			TS4 (X=CH_3)			TS5 (X= CH_3)			TS6 (X=CF_3)			TS7 (X=CCl_3)		
	C1-H3	C4-H3	C1-H3-C4	C1-H3	C4-H3	C1-H3-C4	C1-H3	C4-H3	C1-H3-C4	C2-H7	C8-H7	C2-H7-C8	C1-H5	C8-H5	C1-H5-C8	C2-H4	C5-H4	C2-H4-C5	C2-H4	C5-H4	C2-H4-C5
B3LYP/6-311+G(d,p)	1.282	1.472	178.3	1.351	1.35	179.8	1.278	1.439	176.2	1.282	1.483	178.5	1.271	1.449	174.1	1.307	1.433	176.2	1.3	1.438	173.9
B3LYP/6-311++G(d,p)	1.282	1.472	178.3	1.351	1.35	179.8	1.278	1.439	176.2	1.282	1.483	178.6	1.271	1.448	174.2	1.307	1.432	176.2	1.3	1.438	174
B3LYP/6-311++G(2d,2p)	1.284	1.467	178.5	1.349	1.351	179.7	1.278	1.435	176.1	1.284	1.477	178.8	1.272	1.444	174.1	1.307	1.43	176.4	1.301	1.435	174.1
M06-2X/6-311+G(d,p)	1.273	1.465	176.1	1.346	1.342	178.8	1.278	1.423	179.8	1.271	1.478	179.1	1.266	1.44	175.7	1.299	1.426	177.7	1.294	1.43	178.9
M06-2X/6-311++G(d,p)	1.273	1.465	176.3	1.346	1.341	178.7	1.278	1.423	179.8	1.271	1.478	179.2	1.267	1.439	176	1.299	1.426	177.7	1.294	1.43	179.5
M06-2X/6-311++G(2d,2p)	1.273	1.461	176.4	1.341	1.345	178.7	1.264	1.444	179.6	1.271	1.473	179.6	1.266	1.436	175.7	1.298	1.424	178	1.294	1.428	178.7
ωB97XD/6-311+G(d,p)	1.28	1.456	177.3	1.356	1.331	179	1.289	1.407	178.1	1.278	1.467	179.7	1.276	1.422	175.8	1.307	1.411	177.1	1.304	1.414	177.8
ωB97XD/6-311++G(d,p)	1.28	1.456	177.4	1.356	1.33	179.1	1.288	1.407	178.1	1.278	1.467	179.7	1.276	1.422	176.4	1.308	1.411	177.2	1.304	1.413	177.7
ωB97XD/6-311++G(2d,2p)	1.281	1.451	177.6	1.354	1.332	178.9	1.288	1.405	177.7	1.279	1.462	179.9	1.277	1.417	175.6	1.307	1.41	177.5	1.304	1.412	177.8

Table S5. Relative energy profiles (ΔE) (kcal.mol^{-1}) for the H- abstraction reactions (rn1-rn7) of aldehydes and halogenated aldehydes with $\dot{C}H_3$ radical calculated at all nine levels of theory in gas phase.

Level of theory	Reactions															
	rn1				rn2				rn3				rn4			
	PRC	TS	PC	P	PRC	TS	PC	P	PRC	TS	PC	P	PRC	TS	PC	P
B3LYP/6-311+G(d,p)	0.190	5.547	-16.717	-16.894	-0.206	8.891	-3.475	-3.653	-0.297	4.458	-13.304	-13.434	-0.031	5.663	-15.929	-16.203
B3LYP/6-311++G(d,p)	0.194	5.564	-16.725	-16.886	-0.216	8.871	-3.462	-3.636	-0.343	4.445	-13.186	-13.381	-0.003	5.634	-15.968	-16.183
B3LYP/6-311++G(2d,2p)	0.171	5.760	-16.682	-16.958	-0.213	9.110	-3.429	-3.634	-0.309	4.661	-13.490	-13.651	0.009	5.862	-16.011	-16.197
M06-2X/6-311+G(d,p)	-0.935	8.156	-15.723	-16.044	-0.709	11.267	-2.257	-2.526	-1.536	6.594	-13.141	-12.366	-1.340	7.873	-15.526	-15.242
M06-2X/6-311++G(d,p)	-0.928	8.141	-15.722	-16.041	-0.738	11.232	-2.278	-2.523	-1.564	6.558	-12.852	-12.324	-1.509	7.675	-15.693	-15.233
M06-2X/6-311++G(2d,2p)	-1.099	8.122	-16.001	-16.395	-0.650	11.153	-3.044	-2.689	-1.461	6.659	-13.223	-12.908	-1.640	7.736	-15.948	-15.501
ωB97XD/6-311+G(d,p)	-0.384	5.595	-17.093	-17.125	-0.661	8.550	-3.988	-3.783	-0.947	4.226	-13.542	-13.366	-0.537	5.292	-16.547	-16.242
ωB97XD/6-311++G(d,p)	-0.367	5.594	-17.073	-17.120	-0.668	8.572	-3.987	-3.772	-1.017	4.157	-13.591	-13.375	-0.733	5.193	-16.712	-16.325
ωB97XD/6-311++G(2d,2p)	-0.312	5.840	-17.009	-17.062	-0.516	8.825	-3.855	-3.668	-0.774	-13.603	4.525	-13.477	-0.611	5.494	-16.567	-16.115

Level of theory	Reactions											
	rn5				rn6				rn7			
	PRC	TS	PC	P	PRC	TS	PC	P	PRC	TS	PC	P
B3LYP/6-311+G(d,p)	0.166	9.165	-10.667	-10.821	-0.235	6.064	-12.713	-12.837	-0.169	6.111	-12.403	-12.521
B3LYP/6-311++G(d,p)	0.141	9.148	-10.643	-10.828	-0.272	6.061	-12.641	-12.801	-0.225	6.028	-12.450	-12.478
B3LYP/6-311++G(2d,2p)	0.126	9.428	-10.670	-10.845	-0.255	6.281	-12.737	-12.846	-0.186	6.376	-12.603	-14.099
M06-2X/6-311+G(d,p)	-1.340	10.824	-10.228	-9.291	-1.610	8.210	-12.256	-11.544	-1.975	7.225	-12.158	-10.758
M06-2X/6-311++G(d,p)	-1.511	10.790	-10.228	-9.302	-1.940	8.117	-12.408	-11.521	-2.731	6.883	-12.332	-10.772
M06-2X/6-311++G(2d,2p)	-1.651	10.886	-9.993	-9.494	-1.270	8.120	-12.632	-11.872	-2.040	7.088	-12.655	-12.614
ωB97XD/6-311+G(d,p)	-0.351	8.682	-10.450	-10.161	-0.917	5.497	-13.040	-12.834	-1.525	4.869	-12.803	-12.103
ωB97XD/6-311++G(d,p)	-0.861	8.559	-10.663	-10.167	-1.349	5.435	-13.239	-12.804	-1.724	4.832	-12.984	-12.068
ωB97XD/6-311++G(2d,2p)	-0.745	8.933	-10.702	-10.120	-1.221	5.740	-13.255	-12.735	-1.534	5.308	-12.938	-12.173

Table S6. Relative energy profiles (ΔE) (kcal.mol^{-1}) for the H- abstraction reactions (rn1-rn7) of aldehydes and halogenated aldehydes with $\dot{C}H_3$ radical calculated at all nine levels of theory in water phase.

Level of theory	Reactions															
	rn1				rn2				rn3				rn4			
	PRC	TS	PC	P	PRC	TS	PC	P	PRC	TS	PC	P	PRC	TS	PC	P
B3LYP/6-311+G(d,p)	0.365	6.783	-14.874	-15.129	0.306	10.113	-0.611	-0.811	0.245	5.314	-10.666	-10.853	0.352	6.716	-14.554	-14.706
B3LYP/6-311++G(d,p)	0.380	6.780	-14.868	-15.130	0.296	10.048	-0.574	-0.796	0.211	5.286	-10.644	-10.814	0.355	6.702	-14.589	-14.702
B3LYP/6-311++G(2d,2p)	0.309	6.951	-14.931	-15.211	0.275	10.203	-0.683	-0.895	0.230	5.515	-11.025	-11.187	0.279	6.893	-14.621	-14.733
M06-2X/6-311+G(d,p)	0.016	9.495	-13.845	-14.303	-0.138	12.594	-0.131	0.326	-1.439	7.635	-10.080	-9.714	-0.546	8.732	-14.083	-13.730
M06-2X/6-311++G(d,p)	0.014	9.481	-13.857	-14.309	-0.162	12.559	-0.136	0.331	-0.697	7.594	-10.090	-9.679	-0.521	8.729	-14.078	-13.733
M06-2X/6-311++G(2d,2p)	0.083	9.444	-14.153	-14.656	-0.137	12.401	0.853	0.080	-0.614	7.662	-10.699	-10.358	-0.496	8.751	-14.296	-14.009
ωB97XD/6-311+G(d,p)	0.091	6.857	-15.100	-15.339	-0.168	9.963	-0.826	-0.902	-0.365	5.201	-11.125	-10.739	-0.403	6.236	-15.088	-14.696
ωB97XD/6-311++G(d,p)	0.101	6.854	-15.109	-15.344	-0.154	9.906	-0.841	-0.891	-0.426	5.163	-11.040	-10.748	-0.425	6.243	-14.696	-14.699
ωB97XD/6-311++G(2d,2p)	0.324	7.124	-14.923	-15.279	-	10.115	-0.997	-0.884	-0.175	5.515	-10.926	-10.936	-0.282	6.541	-14.967	-14.590

Level of theory	Reactions											
	rn5				rn6				rn7			
	PRC	TS	PC	P	PRC	TS	PC	P	PRC	TS	PC	P
B3LYP/6-311+G(d,p)	0.348	8.951	-10.478	-10.616	0.233	7.454	-10.422	-10.530	0.178	7.112	-10.639	-10.715
B3LYP/6-311++G(d,p)	0.303	8.928	-10.394	-10.619	0.215	7.386	-10.400	-10.505	0.164	7.063	-10.540	-10.679
B3LYP/6-311++G(2d,2p)	0.377	9.179	-10.558	-10.653	0.199	7.580	-10.355	-10.609	0.161	7.357	-10.858	-10.959
M06-2X/6-311+G(d,p)	-1.094	10.659	-10.180	-9.311	-1.332	9.591	-9.790	-9.132	-2.294	7.994	-10.396	-8.909
M06-2X/6-311++G(d,p)	-1.100	10.735	-10.191	-9.315	-1.367	9.558	-9.787	-9.116	-2.368	7.903	-10.433	-8.885
M06-2X/6-311++G(2d,2p)	-1.088	10.781	-10.309	-9.513	-1.413	9.512	-10.132	-9.524	-2.181	8.089	-10.771	-9.465
ωB97XD/6-311+G(d,p)	-0.460	8.414	-10.460	-9.980	-0.586	6.812	-10.712	-10.478	-1.075	5.972	-10.935	-10.208
ωB97XD/6-311++G(d,p)	-0.462	8.568	-10.468	-9.980	-0.535	6.803	-10.459	-10.455	-1.186	5.909	-11.027	-10.178
ωB97XD/6-311++G(2d,2p)	0.184	8.793	-10.365	-9.939	-0.501	7.020	-10.272	-10.423	-0.994	6.315	-11.279	-10.331

Table S7. Rate constant (k_1 in cm^3 $molecule^{-1}$ s^{-1}) for the reaction (rn1) $HCHO + \dot{C}H_3 \rightarrow H\dot{C}O + CH_4$ in the temperature range 300-1700 K, at 1 atm pressure in gas phase.

T (K)	B3LYP-B1	B3LYP-B2	B3LYP-B3	M062X-B1	M062X-B2	M062X-B3	ωB97XD-B1	ωB97XD-B2	ωB97XD-B3	Literature values					
	TST/Eck	TST/Eck	TST/Eck	TST/Eck	TST/Eck	TST/Eck	TST/Eck	TST/Eck	TST/Eck	Expt[a]	VTST/Eck[b]	CVT/SCT[c]	Expt[d]	Expt[e]	Expt[f]
298	2.14E-15	5.16E-16	6.56E-16	9.24E-18	9.84E-18	1.10E-17	1.77E-16	1.80E-16	1.31E-16						
300	2.22E-15	5.37E-16	6.83E-16	9.65E-18	1.03E-17	1.14E-17	1.83E-16	1.86E-16	1.36E-16	1.59E-17	7.96E-19	2.21E-18	6.25E-18		
400	1.24E-14	3.00E-15	3.87E-15	7.13E-17	7.56E-17	7.68E-17	8.50E-16	8.66E-16	6.51E-16	8.91E-17	2.13E-17	4.63E-17	8.08E-17		
500	4.56E-14	1.10E-14	1.45E-14	3.57E-16	3.79E-16	3.67E-16	2.83E-15	2.89E-15	2.25E-15	3.65E-16	2.20E-16	4.34E-16	3.75E-15	1.28E-15	
600	1.26E-13	3.04E-14	4.10E-14	1.28E-15	1.36E-15	1.28E-15	7.40E-15	7.54E-15	6.04E-15	1.20E-15	1.24E-15	2.45E-15		4.22E-15	
700	2.88E-13	6.95E-14	9.53E-14	3.61E-15	3.81E-15	3.55E-15	1.63E-14	1.66E-14	1.36E-14	3.34E-15	4.78E-15	8.75E-15			
800	5.76E-13	1.39E-13	1.93E-13	8.53E-15	8.99E-15	8.30E-15	3.18E-14	3.23E-14	2.70E-14	8.23E-15	1.41E-14	2.26E-14			2.17 E-14
900	1.04E-12	2.51E-13	3.53E-13	1.77E-14	1.86E-14	1.71E-14	5.64E-14	5.74E-14	4.86E-14	1.84E-14	3.47E-14	8.08E-14			6.40 E-14
1000	1.75E-12	4.21E-13	5.99E-13	3.31E-14	3.48E-14	3.18E-14	9.32E-14	9.49E-14	8.13E-14	3.80E-14	7.44E-14	1.34E-13			5.25 E-14
1100	2.76E-12	6.66E-13	9.54E-13	5.75E-14	6.04E-14	5.50E-14	1.46E-13	1.48E-13	1.28E-13	7.37E-14	1.44E-13				
1200	4.16E-12	1.00E-12	1.45E-12	9.37E-14	9.85E-14	8.95E-14	2.17E-13	2.21E-13	1.93E-13	1.35E-13	2.56E-13	3.70E-13			
1300	6.03E-12	1.45E-12	2.11E-12	1.45E-13	1.53E-13	1.38E-13	3.12E-13	3.18E-13	2.80E-13	2.37E-13	4.27E-13	7.18E-13			
1400	8.44E-12	2.03E-12	2.97E-12	2.16E-13	2.27E-13	2.05E-13	4.35E-13	4.42E-13	3.92E-13	3.99E-13	6.76E-13				
1500	1.15E-11	2.77E-12	4.06E-12	3.10E-13	3.25E-13	2.94E-13	5.89E-13	5.99E-13	5.34E-13	6.50E-13	1.02E-12				
1600	1.53E-11	3.68E-12	5.43E-12	4.31E-13	4.52E-13	4.09E-13	7.80E-13	7.93E-13	7.11E-13	1.03E-12	1.49E-12	2.69E-12			
1700	1.99E-11	4.79E-12	7.09E-12	5.85E-13	6.13E-13	5.54E-13	1.01E-12	1.03E-12	9.27E-13	1.58E-12	2.11E-12				

***B1**- 6-311+G(d,p); **B2**- 6-311++G(d,p); **B3**- 6-311++G(2d,2p)* [a](Choudhury et al., 1989), [b](Nguyen and Nguyen, 2018), [c](Liu et al., 2003), [d](Kerr & Parsonage, 1976), [e](Anastasi, 1983), [f](Manthorne and Pacey, 1978)

Table S8. Rate constant (k_2 in cm^3 $molecule^{-1}$ s^{-1}) for the reaction (rn2) $FCHO + \dot{C}H_3 \rightarrow F\dot{C}O + CH_4$ in the temperature range 300-1700 K, at 1 atm pressure in gas phase.

T (K)	B3LYP-B1	B3LYP-B2	B3LYP-B3	M062X-B1	M062X-B2	M062X-B3	ωB97XD-B1	ωB97XD-B2	ωB97XD-B3	Literature values	
	TST/Eck	TST/Eck	TST/Eck	TST/Eck	TST/Eck	TST/Eck	TST/Eck	TST/Eck	TST/Eck		
298	1.44E-18	1.46E-18	7.85E-19	1.77E-20	1.88E-20	2.83E-20	4.02E-18	1.37E-18	1.16E-18		
300	1.52E-18	1.55E-18	8.32E-19	1.90E-20	2.02E-20	3.03E-20	4.24E-18	1.46E-18	1.22E-18		
400	2.10E-17	2.13E-17	1.14E-17	5.21E-19	5.47E-19	6.89E-19	4.57E-17	1.86E-17	1.31E-17		
500	1.52E-16	1.53E-16	8.31E-17	6.16E-18	6.42E-18	7.44E-18	2.86E-16	1.21E-16	8.33E-17		
600	6.84E-16	6.86E-16	3.80E-16	3.93E-17	4.08E-17	4.53E-17	1.18E-15	5.06E-16	3.49E-16		
700	2.25E-15	2.25E-15	1.26E-15	1.67E-16	1.72E-16	1.86E-16	3.63E-15	1.57E-15	1.09E-15		
800	5.92E-15	5.92E-15	3.37E-15	5.35E-16	5.50E-16	5.84E-16	9.15E-15	3.96E-15	2.79E-15		
900	1.33E-14	1.33E-14	7.66E-15	1.40E-15	1.44E-15	1.51E-15	1.99E-14	8.61E-15	6.13E-15	4.00E-15[a]	1.71E-20[b]
1000	2.67E-14	2.66E-14	1.55E-14	3.17E-15	3.25E-15	3.37E-15	3.88E-14	1.68E-14	1.20E-14	**(with OH)**	**(with NO3)**
1100	4.88E-14	4.86E-14	2.84E-14	6.42E-15	6.57E-15	6.76E-15	6.94E-14	3.00E-14	2.17E-14		
1200	8.31E-14	8.26E-14	4.87E-14	1.19E-14	1.21E-14	1.24E-14	1.16E-13	5.00E-14	3.64E-14		
1300	1.33E-13	1.33E-13	7.85E-14	2.05E-14	2.09E-14	2.13E-14	1.83E-13	7.90E-14	5.80E-14		
1400	2.04E-13	2.03E-13	1.21E-13	3.34E-14	3.40E-14	3.45E-14	2.77E-13	1.19E-13	8.80E-14		
1500	3.01E-13	2.98E-13	1.78E-13	5.18E-14	5.28E-14	5.34E-14	4.03E-13	1.74E-13	1.29E-13		
1600	4.28E-13	4.25E-13	2.55E-13	7.73E-14	7.88E-14	7.93E-14	5.69E-13	2.44E-13	1.82E-13		
1700	5.92E-13	5.87E-13	3.53E-13	1.12E-13	1.13E-13	1.14E-13	7.80E-13	3.35E-13	2.50E-13		

***B1**- 6-311+G(d,p); **B2**- 6-311++G(d,p); **B3**- 6-311++G(2d,2p)* [a](Wallington and Hurley, 1993),[b](Mora-Diez and Boyd, 2002)

Table S9. Rate constant (k_3 in cm^3 $molecule^{-1}$ s^{-1}) for the reaction (rn3) $ClCHO + \dot{C}H_3 \rightarrow Cl\dot{C}O + CH_4$ in the temperature range 300-1700 K, at 1 atm pressure in gas phase.

T (K)	B3LYP-B1	B3LYP-B2	B3LYP-B3	M062X-B1	M062X-B2	M062X-B3	ωB97XD-B1	ωB97XD-B2	ωB97XD-B3	Literature values	
	TST/Eck	TST/Eck	TST/Eck	TST/Eck	TST/Eck	TST/Eck	TST/Eck	TST/Eck	TST/Eck		
298	7.76E-16	7.27E-16	3.22E-15	2.00E-17	2.11E-17	2.32E-17	8.31E-16	1.91E-15	1.18E-15		
300	8.02E-16	7.51E-16	3.33E-15	2.08E-17	2.19E-17	2.41E-17	8.54E-16	1.96E-15	1.22E-15		
400	3.42E-15	3.18E-15	1.47E-14	1.18E-16	1.23E-16	1.26E-16	2.84E-15	6.57E-15	4.38E-15		
500	1.04E-14	9.58E-15	4.62E-14	4.67E-16	4.84E-16	4.81E-16	7.41E-15	1.72E-14	1.21E-14		
600	2.51E-14	2.30E-14	1.14E-13	1.40E-15	1.44E-15	1.41E-15	1.62E-14	3.75E-14	2.77E-14		
700	5.17E-14	4.74E-14	2.40E-13	3.41E-15	3.50E-15	3.42E-15	3.11E-14	7.22E-14	5.51E-14		
800	9.53E-14	8.72E-14	4.50E-13	7.21E-15	7.38E-15	7.19E-15	5.46E-14	1.27E-13	9.91E-14		
900	1.62E-13	1.48E-13	7.75E-13	1.36E-14	1.39E-14	1.36E-14	8.91E-14	2.07E-13	1.65E-13	5.00E-13[a]	1.50E-17[b]
1000	2.58E-13	2.35E-13	1.25E-12	2.38E-14	2.42E-14	2.36E-14	1.37E-13	3.19E-13	2.59E-13	**(with OH)**	**(with NO_3)**
1100	3.90E-13	3.55E-13	1.90E-12	3.88E-14	3.95E-14	3.85E-14	2.03E-13	4.70E-13	3.88E-13		
1200	5.65E-13	5.15E-13	2.78E-12	6.01E-14	6.11E-14	5.96E-14	2.89E-13	6.69E-13	5.59E-13		
1300	7.93E-13	7.22E-13	3.93E-12	8.90E-14	9.04E-14	8.84E-14	3.98E-13	9.22E-13	7.79E-13		
1400	1.08E-12	9.83E-13	5.39E-12	1.27E-13	1.29E-13	1.26E-13	5.34E-13	1.24E-12	1.06E-12		
1500	1.44E-12	1.31E-12	7.20E-12	1.76E-13	1.79E-13	1.75E-13	7.01E-13	1.63E-12	1.40E-12		
1600	1.87E-12	1.70E-12	9.42E-12	2.38E-13	2.42E-13	2.37E-13	9.03E-13	2.09E-12	1.81E-12		
1700	2.39E-12	2.17E-12	1.21E-11	3.15E-13	3.19E-13	3.13E-13	1.14E-12	2.65E-12	2.31E-12		

***B1**- 6-311+G(d,p); **B2**- 6-311++G(d,p); **B3**- 6-311++G(2d,2p)* [a](Libuda et al., 1990), [b](Mora-Diez & Boyd, 2002)

Table S10. Rate constant (k_4 in cm^3 $molecule^{-1}$ s^{-1}) for the reaction (rn4) $CH_3CHO + \dot{C}H_3 \rightarrow CH_3\dot{C}O + CH_4$ in the temperature range 300-1700 K, at 1 atm pressure in gas phase.

T (K)	B3LYP-B1	B3LYP-B2	B3LYP-B3	M062X-B1	M062X-B2	M062X-B3	ωB97XD-B1	ωB97XD-B2	ωB97XD-B3	Literature values				
	TST/Eck	TST/Eck	TST/Eck	TST/Eck	TST/Eck	TST/Eck	TST/Eck	TST/Eck	TST/Eck	Expt[e]	Theoretical[f]	Expt[g]	Expt	Theoretical[h]
298	8.74E-17	2.11E-16	1.74E-16	3.46E-18	2.79E-17	2.32E-17	1.49E-16	5.23E-16	8.85E-16					3.65E-17
300	9.14E-17	2.21E-16	1.81E-16	3.63E-18	2.93E-17	2.43E-17	1.55E-16	5.42E-16	9.19E-16	2.69E-18	1.78E-18		5.70E-18[c]	2.05E-16
400	5.97E-16	1.45E-15	1.22E-15	3.09E-17	2.38E-16	1.88E-16	7.58E-16	2.64E-15	4.75E-15	8.90E-17	3.50E-17	7.527 E-16	9.93E-17[c] 1.01E-16[d]	
500	2.40E-15	5.84E-15	5.04E-15	1.65E-16	1.23E-15	9.55E-16	2.57E-15	8.85E-15	1.68E-14		2.52E-16	4.844 E-15		
600	7.04E-15	1.71E-14	1.51E-14	6.07E-16	4.48E-15	3.44E-15	6.76E-15	2.30E-14	4.56E-14	3.12E-15	1.06E-15	3.203 E-14		
700	1.67E-14	4.08E-14	3.67E-14	1.73E-15	1.27E-14	9.68E-15	1.49E-14	5.04E-14	1.03E-13		3.25E-15	1.25E -13	7.99E-15[a]	1.31E-14
800	3.43E-14	8.38E-14	7.66E-14	4.10E-15	2.99E-14	2.28E-14	2.88E-14	9.72E-14	2.04E-13	1.93E-14	8.04E-15		1.53E-14[a]	
900	6.34E-14	1.55E-13	1.43E-13	8.50E-15	6.17E-14	4.71E-14	5.09E-14	1.71E-13	3.66E-13		1.71E-14			3.79E-14
1000	1.08E-13	2.64E-13	2.47E-13	1.59E-14	1.15E-13	8.82E-14	8.38E-14	2.80E-13	6.11E-13	5.90E-14	3.26E-14		4.70E-14[b]	
1100	1.73E-13	4.22E-13	3.99E-13	2.76E-14	2.00E-13	1.53E-13	1.30E-13	4.35E-13	9.60E-13		5.71E-14		6.78E-14[b]	
1200	2.62E-13	6.41E-13	6.11E-13	4.49E-14	3.24E-13	2.48E-13	1.93E-13	6.44E-13	1.44E-12	1.26E-13	9.38E-14		9.21E-14[b]	
1300	3.82E-13	9.35E-13	8.97E-13	6.93E-14	5.01E-13	3.84E-13	2.76E-13	9.19E-13	2.08E-12		1.46E-13		1.19E-13[b]	
1400	5.39E-13	1.32E-12	1.27E-12	1.03E-13	7.41E-13	5.69E-13	3.83E-13	1.27E-12	2.90E-12		2.18E-13		1.49E-13[b]	
1500	7.37E-13	1.80E-12	1.75E-12	1.47E-13	1.06E-12	8.14E-13	5.16E-13	1.71E-12	3.93E-12	2.77E-13	3.14E-13		1.81E-13[b]	2.23E-13
1600	9.84E-13	2.41E-12	2.35E-12	2.04E-13	1.47E-12	1.13E-12	6.81E-13	2.25E-12	5.21E-12	3.38E-13	4.39E-13		2.14E-13[b]	
1700	1.285E-12	3.143E-12	3.078E-12	2.759E-13	1.989E-12	1.529E-12	8.795E-13	2.91E-12	6.772E-12	4.039E-13	5.976E-13		2.48E-13[b]	

***B1**- 6-311+G(d,p); **B2**- 6-311++G(d,p); **B3**- 6-311++G(2d,2p)-*[a](Liu & Laidler, 1968), [b](Yasunaga et al., 2008), [c](Kerr and Calvert, 1965), [d](Volman and Brinton, 1952) [e](Dodd, 1951), [f](Mendes et al., 2014), [g](Dodd, 1955), [h](Zokaie et al., 2021)

Table S11. Rate constant (k_5 in cm^3 $molecule^{-1}$ s^{-1}) for the reaction (rn5) $CH_3CHO + \dot{C}H_3 \rightarrow CH_2\dot{C}HO + CH_4$ in the temperature range 300-1700 K, at 1 atm pressure in gas phase.

T (K)	B3LYP-B1	B3LYP-B2	B3LYP-B3	M062X-B1	M062X-B2	M062X-B3	ωB97XD-B1	ωB97XD-B2	ωB97XD-B3	Literature values		
	TST/Eck	TST/Eck	TST/Eck	TST/Eck	TST/Eck	TST/Eck	TST/Eck	TST/Eck	TST/Eck	Theoretical[b]	Expt[c]	Theoretical[d]
298	2.20E-19	2.29E-19	1.82E-19	1.41E-20	1.91E-20	2.19E-20	4.33E-19	7.35E-19	4.95E-19			
300	2.35E-19	2.45E-19	1.95E-19	1.53E-20	2.06E-20	2.36E-20	4.58E-19	7.77E-19	5.23E-19	4.10E-22		1.81E-20
400	4.17E-18	4.32E-18	3.52E-18	4.35E-19	5.65E-19	6.10E-19	5.29E-18	8.79E-18	6.25E-18	4.88E-20		3.33E-19
500	3.31E-17	3.42E-17	2.89E-17	4.89E-18	6.24E-18	6.69E-18	3.33E-17	5.45E-17	4.11E-17	1.04E-18		
600	1.56E-16	1.60E-16	1.40E-16	2.94E-17	3.73E-17	4.00E-17	1.35E-16	2.20E-16	1.73E-16	8.98E-18		
700	5.22E-16	5.36E-16	4.82E-16	1.18E-16	1.49E-16	1.61E-16	4.11E-16	6.63E-16	5.42E-16	4.59E-17		
800	1.39E-15	1.43E-15	1.31E-15	3.63E-16	4.56E-16	4.93E-16	1.02E-15	1.64E-15	1.38E-15	1.67E-16	1.25E-17[a]	3.12E-16
900	3.15E-15	3.23E-15	3.02E-15	9.16E-16	1.15E-15	1.25E-15	2.19E-15	3.50E-15	3.01E-15	4.79E-16		
1000	6.33E-15	6.49E-15	6.14E-15	2.01E-15	2.52E-15	2.74E-15	4.21E-15	6.71E-15	5.88E-15	1.16E-15	3.88E-14	1.92E-15
1100	1.16E-14	1.19E-14	1.14E-14	3.96E-15	4.95E-15	5.42E-15	7.44E-15	1.18E-14	1.05E-14	2.48E-15	6.42E-14	
1200	1.97E-14	2.02E-14	1.96E-14	7.16E-15	8.96E-15	9.83E-15	1.23E-14	1.96E-14	1.76E-14	4.79E-15	9.77E-14	
1300	3.17E-14	3.24E-14	3.17E-14	1.21E-14	1.51E-14	1.67E-14	1.93E-14	3.07E-14	2.79E-14	8.57E-15	1.39E-13	
1400	4.85E-14	4.97E-14	4.89E-14	1.94E-14	2.42E-14	2.67E-14	2.89E-14	4.59E-14	4.23E-14	1.44E-14	1.89E-13	
1500	7.14E-14	7.31E-14	7.24E-14	2.97E-14	3.71E-14	4.10E-14	4.18E-14	6.63E-14	6.16E-14	2.30E-14	2.46E-13	
1600	1.02E-13	1.04E-13	1.04E-13	4.37E-14	5.45E-14	6.04E-14	5.86E-14	9.29E-14	8.69E-14	3.51E-14	3.11E-13	5.22E-14
1700	1.40E-13	1.44E-13	1.44E-13	6.22E-14	7.76E-14	8.62E-14	7.99E-14	1.27E-13	1.19E-13	5.18E-14	3.81E-13	

******B1- 6-311+G(d,p); **B2**- 6-311++G(d,p); **B3**- 6-311++G(2d,2p)* [a](Liu & Laidler, 1968) [b](Mendes et al., 2014), [c](Yasunaga et al., 2008), [d](Zokaie et al., 2021)

Table S12. Rate constant (k_6 in cm^3 $molecule^{-1}$ s^{-1}) for the reaction (rn6) $CF_3CHO + \dot{C}H_3 \rightarrow CF_3\dot{C}O + CH_4$ in the temperature range 300-1700 K, at 1 atm pressure in gas phase.

T (K)	B3LYP-B1	B3LYP-B2	B3LYP-B3	M062X-B1	M062X-B2	M062X-B3	ωB97XD-B1	ωB97XD-B2	ωB97XD-B3	Literature values	
	TST/Eck	TST/Eck	TST/Eck	TST/Eck	TST/Eck	TST/Eck	TST/Eck	TST/Eck	TST/Eck		
298	1.66E-16	1.19E-16	2.25E-16	2.72E-18	4.64E-18	1.38E-17	9.97E-17	1.50E-16	9.21E-17		
300	1.74E-16	1.24E-16	2.35E-16	2.84E-18	4.86E-18	1.44E-17	1.03E-16	1.55E-16	9.54E-17		
400	1.14E-15	8.11E-16	1.57E-15	2.25E-17	3.84E-17	1.14E-16	4.78E-16	7.15E-16	4.59E-16		
500	4.75E-15	3.37E-15	6.75E-15	1.20E-16	2.03E-16	6.07E-16	1.60E-15	2.38E-15	1.59E-15		
600	1.45E-14	1.02E-14	2.11E-14	4.48E-16	7.56E-16	2.28E-15	4.18E-15	6.21E-15	4.29E-15		
700	3.56E-14	2.51E-14	5.28E-14	1.30E-15	2.19E-15	6.63E-15	9.24E-15	1.37E-14	9.68E-15		
800	7.53E-14	5.31E-14	1.13E-13	3.14E-15	5.28E-15	1.61E-14	1.80E-14	2.66E-14	1.92E-14		
900	1.42E-13	1.00E-13	2.17E-13	6.64E-15	1.11E-14	3.40E-14	3.21E-14	4.72E-14	3.47E-14	9.5E-14[a]	5.5E-13[b]
1000	2.48E-13	1.74E-13	3.81E-13	1.26E-14	2.11E-14	6.48E-14	5.30E-14	7.80E-14	5.81E-14	**(with OH)**	**(with OH)**
1100	4.03E-13	2.83E-13	6.25E-13	2.22E-14	3.71E-14	1.14E-13	8.29E-14	1.22E-13	9.17E-14		
1200	6.22E-13	4.37E-13	9.72E-13	3.65E-14	6.10E-14	1.88E-13	1.24E-13	1.81E-13	1.38E-13		
1300	9.19E-13	6.45E-13	1.45E-12	5.71E-14	9.52E-14	2.94E-13	1.78E-13	2.60E-13	2.00E-13		
1400	1.31E-12	9.19E-13	2.07E-12	8.54E-14	1.42E-13	4.41E-13	2.47E-13	3.62E-13	2.80E-13		
1500	1.81E-12	1.27E-12	2.88E-12	1.23E-13	2.05E-13	6.37E-13	3.35E-13	4.90E-13	3.81E-13		
1600	2.44E-12	1.71E-12	3.90E-12	1.72E-13	2.87E-13	8.92E-13	4.43E-13	6.48E-13	5.06E-13		
1700	3.22E-12	2.25E-12	5.16E-12	2.35E-13	3.91E-13	1.22E-12	5.74E-13	8.40E-13	6.60E-13		

******B1- 6-311+G(d,p); **B2**- 6-311++G(d,p); **B3**- 6-311++G(2d,2p)* [a](Chandra et al., 2001)[b](Scollard et al., 1993)

Table S13. Rate constant (k_7 in cm^3 $molecule^{-1}$ s^{-1}) for the reaction (rn7) $CCl_3CHO + \dot{C}H_3 \rightarrow CCl_3\dot{C}O + CH_4$ in the temperature range 300-1700 K, at 1 atm pressure in gas phase.

T (K)	B3LYP-B1	B3LYP-B2	B3LYP-B3	M062X-B1	M062X-B2	M062X-B3	ωB97XD-B1	ωB97XD-B2	ωB97XD-B3	Literature values	
	TST/Eck	TST/Eck	TST/Eck	TST/Eck	TST/Eck	TST/Eck	TST/Eck	TST/Eck	TST/Eck		
298	6.85E-17	1.10E-16	8.30E-17	6.12E-18	1.33E-17	6.80E-17	2.07E-16	2.30E-16	1.45E-16		
300	7.16E-17	1.15E-16	8.68E-17	6.37E-18	1.39E-17	7.08E-17	2.13E-16	2.37E-16	1.50E-16		
400	4.89E-16	7.74E-16	6.21E-16	4.08E-17	8.67E-17	4.50E-16	8.57E-16	9.44E-16	6.62E-16		
500	2.09E-15	3.26E-15	2.77E-15	1.80E-16	3.72E-16	1.98E-15	2.57E-15	2.81E-15	2.14E-15		
600	6.47E-15	9.99E-15	8.86E-15	5.88E-16	1.18E-15	6.45E-15	6.25E-15	6.78E-15	5.49E-15		
700	1.61E-14	2.46E-14	2.26E-14	1.54E-15	3.03E-15	1.69E-14	1.30E-14	1.41E-14	1.20E-14		
800	3.42E-14	5.21E-14	4.92E-14	3.44E-15	6.64E-15	3.77E-14	2.44E-14	2.62E-14	2.31E-14		
900	6.50E-14	9.86E-14	9.53E-14	6.80E-15	1.30E-14	7.48E-14	4.19E-14	4.48E-14	4.08E-14	5.7E-13[a] **(with OH)**	1.6E-12[b] **(with OH)**
1000	1.13E-13	1.72E-13	1.69E-13	1.23E-14	2.32E-14	1.35E-13	6.74E-14	7.19E-14	6.71E-14		
1100	1.85E-13	2.79E-13	2.79E-13	2.07E-14	3.86E-14	2.28E-13	1.03E-13	1.10E-13	1.04E-13		
1200	2.86E-13	4.31E-13	4.37E-13	3.29E-14	6.08E-14	3.63E-13	1.51E-13	1.60E-13	1.55E-13		
1300	4.24E-13	6.37E-13	6.53E-13	4.98E-14	9.15E-14	5.51E-13	2.13E-13	2.26E-13	2.22E-13		
1400	6.06E-13	9.08E-13	9.39E-13	7.26E-14	1.33E-13	8.05E-13	2.92E-13	3.10E-13	3.09E-13		
1500	8.39E-13	1.26E-12	1.31E-12	1.02E-13	1.86E-13	1.14E-12	3.91E-13	4.14E-13	4.18E-13		
1600	1.13E-12	1.69E-12	1.78E-12	1.40E-13	2.54E-13	1.56E-12	5.12E-13	5.41E-13	5.52E-13		
1700	1.49E-12	2.23E-12	2.36E-12	1.88E-13	3.38E-13	2.09E-12	6.58E-13	6.95E-13	7.14E-13		

***B1**- 6-311+G(d,p); **B2**- 6-311++G(d,p); **B3**- 6-311++G(2d,2p)* [a](Chandra et al., 2001), [b](Scollard et al., 1993)

Table S14. Rate constant (k_1-w in cm^3 $molecule^{-1}$ s^{-1}) for the reaction (rn1) $HCHO + \dot{C}H_3 \rightarrow H\dot{C}O + CH_4$ in the temperature range 300-1700 K, at 1 atm pressure in water phase.

T (K)	B3LYP-B1	B3LYP-B2	B3LYP-B3	M062X-B1	M062X-B2	M062X-B3	ωB97XD-B1	ωB97XD-B2	ωB97XD-B3
	TST/Eck	TST/Eck	TST/Eck	TST/Eck	TST/Eck	TST/Eck	TST/Eck	TST/Eck	TST/Eck
298	4.78E-17	4.99E-17	7.31E-17	7.77E-19	7.88E-19	9.971E-19	2.53E-17	2.53E-17	1.62E-17
300	5.01E-17	5.22E-17	7.65E-17	8.14E-19	8.26E-19	1.041E-18	2.64E-17	2.63E-17	1.69E-17
400	3.73E-16	3.89E-16	5.72E-16	7.39E-18	7.47E-18	8.358E-18	1.58E-16	1.57E-16	1.03E-16
500	1.71E-15	1.78E-15	2.66E-15	4.54E-17	4.58E-17	4.807E-17	6.46E-16	6.43E-16	4.32E-16
600	5.57E-15	5.81E-15	8.82E-15	1.92E-16	1.93E-16	1.954E-16	1.97E-15	1.96E-15	1.35E-15
700	1.44E-14	1.50E-14	2.31E-14	6.11E-16	6.14E-16	6.088E-16	4.90E-15	4.87E-15	3.42E-15
800	3.16E-14	3.30E-14	5.15E-14	1.59E-15	1.60E-15	1.56E-15	1.05E-14	1.04E-14	7.41E-15
900	6.18E-14	6.44E-14	1.02E-13	3.56E-15	3.57E-15	3.454E-15	2.00E-14	1.98E-14	1.43E-14
1000	1.10E-13	1.15E-13	1.83E-13	7.11E-15	7.12E-15	6.846E-15	3.51E-14	3.48E-14	2.55E-14
1100	1.83E-13	1.91E-13	3.06E-13	1.30E-14	1.30E-14	1.244E-14	5.77E-14	5.72E-14	4.22E-14
1200	2.88E-13	3.00E-13	4.85E-13	2.22E-14	2.22E-14	2.111E-14	8.98E-14	8.90E-14	6.62E-14
1300	4.33E-13	4.51E-13	7.32E-13	3.57E-14	3.57E-14	3.384E-14	1.34E-13	1.33E-13	9.93E-14
1400	6.27E-13	6.53E-13	1.06E-12	5.47E-14	5.47E-14	5.18E-14	1.92E-13	1.90E-13	1.43E-13
1500	8.78E-13	9.14E-13	1.50E-12	8.08E-14	8.07E-14	7.625E-14	2.68E-13	2.65E-13	2.01E-13
1600	1.196E-12	1.245E-12	2.048E-12	1.153E-13	1.152E-13	1.086E-13	3.628E-13	3.592E-13	2.731E-13
1700	1.592E-12	1.657E-12	2.735E-12	1.599E-13	1.597E-13	1.504E-13	4.807E-13	4.76E-13	3.634E-13

***B1**- 6-311+G(d,p); **B2**- 6-311++G(d,p); **B3**- 6-311++G(2d,2p)*

Table S15. Rate constant (k_2-w in cm^3 $molecule^{-1}$ s^{-1}) for the reaction (rn2) $FCHO + \dot{C}H_3 \rightarrow F\dot{C}O + CH_4$ in the temperature range 300-1700 K, at 1 atm pressure in water phase.

T (K)	B3LYP-B1	B3LYP-B2	B3LYP-B3	M062X-B1	M062X-B2	M062X-B3	ωB97XD-B1	ωB97XD-B2	ωB97XD-B3
	TST/Eck	TST/Eck	TST/Eck	TST/Eck	TST/Eck	TST/Eck	TST/Eck	TST/Eck	TST/Eck
298	1.33E-19	4.11E-19	4.15E-19	1.63E-21	1.71E-21	2.908E-21	1.32E-19	1.90E-19	1.08E-19
300	1.43E-19	4.42E-19	4.46E-19	1.79E-21	1.87E-21	3.167E-21	1.41E-19	2.03E-19	1.15E-19
400	3.38E-18	1.04E-17	1.01E-17	9.20E-20	9.54E-20	1.314E-19	2.62E-18	3.76E-18	2.07E-18
500	3.39E-17	1.03E-16	1.01E-16	1.57E-18	1.62E-18	2.024E-18	2.31E-17	3.30E-17	1.82E-17
600	1.90E-16	5.77E-16	5.66E-16	1.28E-17	1.31E-17	1.551E-17	1.20E-16	1.71E-16	9.49E-17
700	7.29E-16	2.21E-15	2.18E-15	6.44E-17	6.57E-17	7.504E-17	4.38E-16	6.21E-16	3.48E-16
800	2.16E-15	6.53E-15	6.50E-15	2.34E-16	2.38E-16	2.656E-16	1.25E-15	1.77E-15	9.98E-16
900	5.32E-15	1.61E-14	1.61E-14	6.79E-16	6.88E-16	7.533E-16	3.00E-15	4.24E-15	2.40E-15
1000	1.15E-14	3.46E-14	3.48E-14	1.66E-15	1.68E-15	1.815E-15	6.32E-15	8.91E-15	5.08E-15
1100	2.22E-14	6.70E-14	6.78E-14	3.58E-15	3.62E-15	3.866E-15	1.20E-14	1.70E-14	9.70E-15
1200	3.97E-14	1.20E-13	1.22E-13	7.00E-15	7.07E-15	7.475E-15	2.12E-14	2.98E-14	1.71E-14
1300	6.65E-14	2.00E-13	2.04E-13	1.26E-14	1.27E-14	1.338E-14	3.51E-14	4.93E-14	2.84E-14
1400	1.056E-13	3.174E-13	3.246E-13	2.14E-14	2.156E-14	2.25E-14	5.512E-14	7.745E-14	4.476E-14
1500	1.603E-13	4.816E-13	4.94E-13	3.437E-14	3.459E-14	3.591E-14	8.295E-14	1.165E-13	6.748E-14
1600	2.34E-13	7.04E-13	7.24E-13	5.28E-14	5.31E-14	5.488E-14	1.20E-13	1.69E-13	9.81E-14
1700	3.32E-13	9.97E-13	1.03E-12	7.81E-14	7.85E-14	8.084E-14	1.69E-13	2.38E-13	1.38E-13

**B1- 6-311+G(d,p); B2- 6-311++G(d,p); B3- 6-311++G(2d,2p)*

Table S16. Rate constant (k_3-w in cm^3 $molecule^{-1}$ s^{-1}) for the reaction (rn3) $ClCHO + \dot{C}H_3 \rightarrow Cl\dot{C}O + CH_4$ in the temperature range 300-1700 K, at 1 atm pressure in water phase.

T (K)	B3LYP-B1	B3LYP-B2	B3LYP-B3	M062X-B1	M062X-B2	M062X-B3	ωB97XD-B1	ωB97XD-B2	ωB97XD-B3
	TST/Eck	TST/Eck	TST/Eck	TST/Eck	TST/Eck	TST/Eck	TST/Eck	TST/Eck	TST/Eck
298	6.56E-16	5.90E-16	5.42E-16	3.18E-18	3.40E-18	4.23E-18	2.70E-16	1.48E-16	1.77E-16
300	6.83E-16	6.14E-16	5.64E-16	3.33E-18	3.56E-18	4.41E-18	2.79E-16	1.53E-16	1.83E-16
400	3.86E-15	3.44E-15	3.24E-15	2.71E-17	2.86E-17	3.19E-17	1.24E-15	6.67E-16	8.62E-16
500	1.42E-14	1.26E-14	1.22E-14	1.39E-16	1.45E-16	1.54E-16	3.98E-15	2.12E-15	2.91E-15
600	3.94E-14	3.47E-14	3.44E-14	4.96E-16	5.14E-16	5.36E-16	1.01E-14	5.35E-15	7.68E-15
700	9.00E-14	7.90E-14	7.98E-14	1.38E-15	1.42E-15	1.47E-15	2.18E-14	1.15E-14	1.70E-14
800	1.79E-13	1.57E-13	1.61E-13	3.21E-15	3.30E-15	3.39E-15	4.16E-14	2.18E-14	3.33E-14
900	3.24E-13	2.83E-13	2.94E-13	6.56E-15	6.73E-15	6.884E-15	7.28E-14	3.81E-14	5.93E-14
1000	5.42E-13	4.72E-13	4.96E-13	1.22E-14	1.24E-14	1.27E-14	1.19E-13	6.20E-14	9.82E-14
1100	8.53E-13	7.43E-13	7.88E-13	2.08E-14	2.13E-14	2.17E-14	1.83E-13	9.55E-14	1.54E-13
1200	1.281E-12	1.115E-12	1.191E-12	3.36E-14	3.43E-14	3.50E-14	2.711E-13	1.41E-13	2.295E-13
1300	1.85E-12	1.609E-12	1.73E-12	5.17E-14	5.26E-14	5.37E-14	3.86E-13	2.006E-13	3.299E-13
1400	2.58E-12	2.25E-12	2.43E-12	7.61E-14	7.76E-14	7.91E-14	5.34E-13	2.77E-13	4.59E-13
1500	3.51E-12	3.05E-12	3.32E-12	1.08E-13	1.10E-13	1.13E-13	7.18E-13	3.72E-13	6.22E-13
1600	4.66E-12	4.04E-12	4.42E-12	1.50E-13	1.52E-13	1.56E-13	9.45E-13	4.90E-13	8.24E-13
1700	6.06E-12	5.25E-12	5.76E-12	2.02E-13	2.05E-13	2.09E-13	1.22E-12	6.31E-13	1.07E-12

**B1- 6-311+G(d,p); B2- 6-311++G(d,p); B3- 6-311++G(2d,2p)*

Table S17. Rate constant (k_4-w in cm^3 $molecule^{-1}$ s^{-1}) for the reaction (rn4) $CH_3CHO + \dot{C}H_3 \rightarrow CH_3\dot{C}O + CH_4$ in the temperature range 300-1700 K, at 1 atm pressure in water phase.

T (K)	B3LYP-B1	B3LYP-B2	B3LYP-B3	M062X-B1	M062X-B2	M062X-B3	ωB97XD-B1	ωB97XD-B2	ωB97XD-B3
	TST/Eck	TST/Eck	TST/Eck	TST/Eck	TST/Eck	TST/Eck	TST/Eck	TST/Eck	TST/Eck
298	2.73E-17	3.32E-17	6.90E-17	7.87E-18	6.58E-18	6.23E-18	2.11E-16	1.80E-16	1.05E-16
300	2.86E-17	3.49E-17	7.25E-17	8.26E-18	6.91E-18	6.53E-18	2.19E-16	1.88E-16	1.09E-16
400	2.42E-16	2.95E-16	6.20E-16	8.00E-17	6.67E-17	5.90E-17	1.34E-15	1.15E-15	6.91E-16
500	1.19E-15	1.44E-15	3.10E-15	4.90E-16	4.08E-16	3.50E-16	5.42E-15	4.64E-15	2.90E-15
600	4.03E-15	4.89E-15	1.07E-14	2.03E-15	1.69E-15	1.43E-15	1.62E-14	1.39E-14	8.98E-15
700	1.07E-14	1.30E-14	2.90E-14	6.36E-15	5.28E-15	4.43E-15	3.95E-14	3.38E-14	2.24E-14
800	2.39E-14	2.90E-14	6.56E-14	1.63E-14	1.35E-14	1.13E-14	8.29E-14	7.10E-14	4.80E-14
900	4.72E-14	5.73E-14	1.31E-13	3.59E-14	2.98E-14	2.48E-14	1.56E-13	1.34E-13	9.17E-14
1000	8.48E-14	1.03E-13	2.38E-13	7.07E-14	5.86E-14	4.87E-14	2.70E-13	2.32E-13	1.61E-13
1100	1.42E-13	1.72E-13	4.02E-13	1.28E-13	1.06E-13	8.80E-14	4.38E-13	3.76E-13	2.64E-13
1200	2.24E-13	2.72E-13	6.39E-13	2.16E-13	1.79E-13	1.48E-13	6.75E-13	5.79E-13	4.11E-13
1300	3.38E-13	4.10E-13	9.69E-13	3.44E-13	2.85E-13	2.36E-13	9.95E-13	8.54E-13	6.11E-13
1400	4.90E-13	5.94E-13	1.41E-12	5.24E-13	4.34E-13	3.59E-13	1.42E-12	1.22E-12	8.76E-13
1500	6.87E-13	8.33E-13	1.99E-12	7.67E-13	6.35E-13	5.26E-13	1.96E-12	1.68E-12	1.22E-12
1600	9.38E-13	1.14E-12	2.73E-12	1.09E-12	9.00E-13	7.46E-13	2.63E-12	2.26E-12	1.65E-12
1700	1.25E-12	1.51E-12	3.65E-12	1.50E-12	1.24E-12	1.03E-12	3.47E-12	2.98E-12	2.18E-12

**B1- 6-311+G(d,p); B2- 6-311++G(d,p); B3- 6-311++G(2d,2p)*

Table S18. Rate constant (k_5-w in cm^3 $molecule^{-1}$ s^{-1}) for the reaction (rn5) $CH_3CHO + \dot{C}H_3 \rightarrow CH_2\dot{C}HO + CH_4$ in the temperature range 300-1700 K, at 1 atm pressure in water phase.

T (K)	B3LYP-B1	B3LYP-B2	B3LYP-B3	M062X-B1	M062X-B2	M062X-B3	ωB97XD-B1	ωB97XD-B2	ωB97XD-B3
	TST/Eck	TST/Eck	TST/Eck	TST/Eck	TST/Eck	TST/Eck	TST/Eck	TST/Eck	TST/Eck
298	2.19E-19	2.69E-19	2.17E-19	7.37E-20	2.82E-20	3.65E-20	1.46E-18	3.83E-19	4.15E-19
300	2.35E-19	2.89E-19	2.32E-19	7.97E-20	3.05E-20	3.94E-20	1.55E-18	4.06E-19	4.40E-19
400	4.41E-18	5.40E-18	4.41E-18	2.29E-18	8.78E-19	1.06E-18	1.88E-17	5.01E-18	5.56E-18
500	3.51E-17	4.28E-17	3.60E-17	2.56E-17	9.84E-18	1.17E-17	1.18E-16	3.21E-17	3.69E-17
600	1.63E-16	1.99E-16	1.72E-16	1.53E-16	5.90E-17	6.96E-17	4.79E-16	1.31E-16	1.55E-16
700	5.40E-16	6.57E-16	5.83E-16	6.12E-16	2.36E-16	2.79E-16	1.44E-15	3.97E-16	4.82E-16
800	1.43E-15	1.73E-15	1.56E-15	1.87E-15	7.22E-16	8.51E-16	3.56E-15	9.82E-16	1.22E-15
900	3.20E-15	3.89E-15	3.56E-15	4.70E-15	1.82E-15	2.15E-15	7.58E-15	2.10E-15	2.64E-15
1000	6.37E-15	7.74E-15	7.18E-15	1.03E-14	3.98E-15	4.71E-15	1.45E-14	4.03E-15	5.14E-15
1100	1.16E-14	1.41E-14	1.32E-14	2.02E-14	7.83E-15	9.27E-15	2.55E-14	7.10E-15	9.16E-15
1200	1.96E-14	2.38E-14	2.25E-14	3.64E-14	1.42E-14	1.68E-14	4.21E-14	1.17E-14	1.53E-14
1300	3.13E-14	3.80E-14	3.62E-14	6.15E-14	2.39E-14	2.84E-14	6.58E-14	1.83E-14	2.41E-14
1400	4.78E-14	5.79E-14	5.56E-14	9.83E-14	3.82E-14	4.55E-14	9.84E-14	2.75E-14	3.64E-14
1500	7.00E-14	8.48E-14	8.19E-14	1.50E-13	5.84E-14	6.96E-14	1.42E-13	3.96E-14	5.28E-14
1600	9.92E-14	1.20E-13	1.17E-13	2.21E-13	8.59E-14	1.02E-13	1.98E-13	5.54E-14	7.43E-14
1700	1.37E-13	1.66E-13	1.61E-13	3.14E-13	1.22E-13	1.46E-13	2.70E-13	7.54E-14	1.02E-13

**B1- 6-311+G(d,p); B2- 6-311++G(d,p); B3- 6-311++G(2d,2p)*

Table S19. Rate constant (k_6-w in cm^3 $molecule^{-1}$ s^{-1}) for the reaction (rn6) $CF_3CHO + \dot{C}H_3 \rightarrow CF_3\dot{C}O + CH_4$ in the temperature range 300-1700 K, at 1 atm pressure in water phase.

T (K)	B3LYP-B1	B3LYP-B2	B3LYP-B3	M062X-B1	M062X-B2	M062X-B3	ωB97XD-B1	ωB97XD-B2	ωB97XD-B3
	TST/Eck	TST/Eck	TST/Eck	TST/Eck	TST/Eck	TST/Eck	TST/Eck	TST/Eck	TST/Eck
298	6.03E-18	2.62E-17	1.65E-17	4.44E-19	5.06E-19	7.79E-19	4.23E-17	4.27E-17	3.48E-17
300	6.34E-18	2.75E-17	1.74E-17	4.70E-19	5.35E-19	8.21E-19	4.41E-17	4.45E-17	3.63E-17
400	5.84E-17	2.53E-16	1.60E-16	6.14E-18	6.96E-18	9.44E-18	2.85E-16	2.86E-16	2.38E-16
500	3.16E-16	1.37E-15	8.78E-16	4.65E-17	5.24E-17	6.69E-17	1.23E-15	1.23E-15	1.05E-15
600	1.16E-15	5.01E-15	3.28E-15	2.23E-16	2.50E-16	3.09E-16	3.89E-15	3.89E-15	3.39E-15
700	3.29E-15	1.42E-14	9.39E-15	7.74E-16	8.67E-16	1.05E-15	9.92E-15	9.90E-15	8.77E-15
800	7.76E-15	3.33E-14	2.24E-14	2.14E-15	2.39E-15	2.87E-15	2.16E-14	2.15E-14	1.94E-14
900	1.60E-14	6.86E-14	4.65E-14	5.02E-15	5.59E-15	6.65E-15	4.20E-14	4.18E-14	3.80E-14
1000	2.98E-14	1.28E-13	8.73E-14	1.04E-14	1.16E-14	1.37E-14	7.46E-14	7.42E-14	6.81E-14
1100	5.13E-14	2.20E-13	1.51E-13	1.95E-14	2.17E-14	2.56E-14	1.24E-13	1.23E-13	1.14E-13
1200	8.31E-14	3.56E-13	2.46E-13	3.40E-14	3.78E-14	4.44E-14	1.94E-13	1.93E-13	1.80E-13
1300	1.28E-13	5.48E-13	3.81E-13	5.58E-14	6.20E-14	7.26E-14	2.91E-13	2.89E-13	2.71E-13
1400	1.89E-13	8.08E-13	5.65E-13	8.70E-14	9.65E-14	1.13E-13	4.19E-13	4.16E-13	3.93E-13
1500	2.70E-13	1.15E-12	8.09E-13	1.30E-13	1.44E-13	1.68E-13	5.86E-13	5.82E-13	5.51E-13
1600	3.73E-13	1.59E-12	1.12E-12	1.88E-13	2.08E-13	2.43E-13	7.98E-13	7.92E-13	7.53E-13
1700	5.04E-13	2.15E-12	1.52E-12	2.63E-13	2.91E-13	3.39E-13	1.06E-12	1.05E-12	1.00E-12

**B1- 6-311+G(d,p); B2- 6-311++G(d,p); B3- 6-311++G(2d,2p)*

Table S20. Rate constant (k_7-w in cm^3 $molecule^{-1}$ s^{-1}) for the reaction (rn7) $CCl_3CHO + \dot{C}H_3 \rightarrow CCl_3\dot{C}O + CH_4$ in the temperature range 300-1700 K, at 1 atm pressurein water phase.

T (K)	B3LYP-B1	B3LYP-B2	B3LYP-B3	M062X-B1	M062X-B2	M062X-B3	ωB97XD-B1	ωB97XD-B2	ωB97XD-B3
	TST/Eck	TST/Eck	TST/Eck	TST/Eck	TST/Eck	TST/Eck	TST/Eck	TST/Eck	TST/Eck
298	9.08E-18	9.99E-18	8.94E-18	5.51E-18	7.07E-18	2.30E-17	3.53E-17	3.99E-17	2.97E-17
300	9.54E-18	1.05E-17	9.40E-18	5.78E-18	7.42E-18	2.41E-17	3.66E-17	4.14E-17	3.09E-17
400	8.59E-17	9.30E-17	8.66E-17	5.18E-17	6.50E-17	2.04E-16	1.93E-16	2.15E-16	1.73E-16
500	4.49E-16	4.81E-16	4.68E-16	2.89E-16	3.56E-16	1.12E-15	7.12E-16	7.82E-16	6.73E-16
600	1.61E-15	1.71E-15	1.72E-15	1.11E-15	1.35E-15	4.27E-15	2.01E-15	2.19E-15	1.99E-15
700	4.44E-15	4.69E-15	4.87E-15	3.25E-15	3.92E-15	1.26E-14	4.70E-15	5.08E-15	4.80E-15
800	1.03E-14	1.08E-14	1.15E-14	7.91E-15	9.47E-15	3.07E-14	9.58E-15	1.03E-14	1.01E-14
900	2.08E-14	2.18E-14	2.36E-14	1.67E-14	1.99E-14	6.53E-14	1.76E-14	1.89E-14	1.89E-14
1000	3.83E-14	4.00E-14	4.41E-14	3.20E-14	3.79E-14	1.25E-13	3.00E-14	3.20E-14	3.28E-14
1100	6.53E-14	6.81E-14	7.59E-14	5.62E-14	6.63E-14	2.21E-13	4.81E-14	5.11E-14	5.33E-14
1200	1.05E-13	1.09E-13	1.23E-13	9.26E-14	1.09E-13	3.65E-13	7.32E-14	7.76E-14	8.21E-14
1300	1.60E-13	1.66E-13	1.89E-13	1.45E-13	1.70E-13	5.73E-13	1.07E-13	1.13E-13	1.21E-13
1400	2.35E-13	2.44E-13	2.80E-13	2.17E-13	2.54E-13	8.60E-13	1.51E-13	1.60E-13	1.73E-13
1500	3.33E-13	3.45E-13	3.99E-13	3.13E-13	3.66E-13	1.24E-12	2.07E-13	2.19E-13	2.39E-13
1600	4.58E-13	4.75E-13	5.53E-13	4.38E-13	5.11E-13	1.75E-12	2.77E-13	2.92E-13	3.23E-13
1700	6.15E-13	6.37E-13	7.46E-13	5.97E-13	6.95E-13	2.38E-12	3.63E-13	3.82E-13	4.26E-13

**B1- 6-311+G(d,p); B2- 6-311++G(d,p); B3- 6-311++G(2d,2p)*

Conflicts of Interest
The authors confirm that there is no conflict of interest to declare for this publication.

Acknowledgments
Authors GP and SY are thankful to the GRG Institutions and DST-CURIE, for the infrastructure provided.

AI Disclosure
The author(s) declare that no assistance is taken from generative AI to write this article.

References

Anastasi, C. (1983). Reaction of methyl radicals with formaldehyde in the range 500⩽ T/K⩽ 603. *Journal of the Chemical Society, Faraday Transactions 1: Physical Chemistry in Condensed Phases*, *79*(3), 749-753.

Atkinson, R., & Arey, J. (2003). Atmospheric degradation of volatile organic compounds. *Chemical Reviews*, *103*(12), 4605-4638.

Basch, H., & Hoz, S. (1997). Ab initio study of hydrogen abstraction reactions. *The Journal of Physical Chemistry A*, *101*(24), 4416-4431.

Berney, C.V. (1969). Spectroscopy of CF3COZ compounds—III: Vibrational spectrum and barrier to internal rotation of trifluoroacetaldehyde. *Spectrochimica Acta Part A: Molecular Spectroscopy*, *25*(4), 793-809.

Beukes, J.A., D'Anna, B., Bakken, V., & Nielsen, C.J. (2000). Experimental and theoretical study of the F, Cl and Br reactions with formaldehyde and acetaldehyde. *Physical Chemistry Chemical Physics*, *2*(18), 4049-4060.

Buszek, R.J., Francisco, J.S., & Anglada, J.M. (2011). Water effects on atmospheric reactions. *International Reviews in Physical Chemistry*, *30*(3), 335-369.

Canneaux, S., Bohr, F., & Henon, E. (2014). KiSThelP: a program to predict thermodynamic properties and rate constants from quantum chemistry results. *Journal of Computational Chemistry*, *35*(1), 82-93.

Cao, F., Shi, G., Song, J., Tian, P., & Li, Z. (2021). Kinetics of the reactions of methyl radical with hydrogen, methyl and ethyl peroxides. *ChemistrySelect*, *6*(7), 1548-1554.

Carr, S., Shallcross, D.E., Canosa-Mas, C.E., Wenger, J.C., Sidebottom, H.W., Treacy, J.J., & Wayne, R.P. (2003). A kinetic and mechanistic study of the gas-phase reactions of OH radicals and Cl atoms with some halogenated acetones and their atmospheric implications. *Physical Chemistry Chemical Physics, 5*(18), 3874-3883.

Chai, J.-D., & Head-Gordon, M. (2008). Long-range corrected hybrid density functionals with damped atom–atom dispersion corrections. *Physical Chemistry Chemical Physics, 10*(44), 6615-6620.

Chandra, A.K., Uchimaru, T., & Sugie, M. (2001). Kinetics of hydrogen abstraction reactions of CF_3CHO, CF_2ClCHO, $CFCl_2CHO$ and CCl_3CHO with OH radicals: an ab initio study. *Physical Chemistry Chemical Physics*, *3*(18), 3961-3966.

Chase, M.W. (1998). NIST-JANAF thermochemical tables. *Journal of Physical and Chemical Reference Data*, *28*, 1951.

Chen, H., Liu, P., Wang, Q., Huang, R., & Sarwar, G. (2024). Impact and pathway of halogens on atmospheric oxidants in coastal city clusters in the yangtze river delta region in China. *Atmospheric Pollution Research*, *15*(2), 101979.

Chiappero, M.S., Malanca, F.E., Argüello, G.A., Wooldridge, S.T., Hurley, M.D., Ball, J.C., Wallington, T.J., Waterland, R.L, Buck, R.C. (2006). Atmospheric chemistry of perfluoroaldehydes ($C_xF_{2x+1}CHO$) and fluorotelomer aldehydes ($C_xF_{2x+1}CH_2CHO$): quantification of the important role of photolysis. *The Journal of Physical Chemistry A, 110*(43), 11944-11953.

Choudhury, T.K., Sanders, W., & Lin, M.-C. (1989). A shock tube and modeling study of the methyl+ formaldehyde reaction at high temperatures. *The Journal of Physical Chemistry, 93*(13), 5143-5147.

Dodd, R. (1951). Rate constants in the high temperature photolysis of acetaldehyde. *Transactions of the Faraday Society, 47*, 56-62.

Dodd, R. (1955). The reaction of methyl radicals with acetaldehyde. *Canadian Journal of Chemistry, 33*(4), 699-704.

Dong, Z., Xie, C., & Long, B. (2025). Reaction between perfluoroaldehydes and hydroperoxy radical in the atmosphere: reaction mechanisms, reaction kinetics modelling, and atmospheric implications. *EGUsphere*, *2025*, 1-23.

Eckart, C. (1930). The penetration of a potential barrier by electrons. *Physical Review, 35*(11), 1303. https://doi.org/10.1103/PhysRev.35.1303.

Espinosa-García, J., del Valle, F.O., & Corchado, J.C. (1994). Transition state theory and Eckart's tunnelling factor: a good approximation for the calculation of bimolecular rate constants?. *Chemical Physics*, *183*(1), 95-100.

Farahani, P., Maeda, S., Francisco, J.S., & Lundberg, M. (2015). Mechanisms for the breakdown of halomethanes through reactions with ground-state cyano radicals. *ChemPhysChem*, *16*(1), 181-190.

Fernández-Ramos, A., Miller, J.A., Klippenstein, S.J., & Truhlar, D.G. (2006). Modeling the kinetics of bimolecular reactions. *Chemical Reviews, 106*(11), 4518-4584.

Francisco, J. (1992). An examination of substituent effects on the reaction of OH radicals with HXCO (where X= H, F, and C_l). *The Journal of Chemical Physics, 96*(10), 7597-7602.

Frisch, M.J., Trucks, G.W., Schlegel, H.B., Scuseria, G.E., Robb, M.A., Cheeseman, J.R., & Fox, D.J. (2010). Gaussian 09, revision C. O1, Gaussian. *Inc, Walling-Ford, CT*.

Gao, Y., Zhao, Y., Guan, Q., & Wang, F. (2020). Ab initio kinetics predictions for the role of pre-reaction complexes in hydrogen abstraction from 2-butanone by OH radicals. *RSC Advances*, *10*(55), 33205-33212.

Gonzalez, C., & Schlegel, H.B. (1989). An improved algorithm for reaction path following. *The Journal of Chemical Physics, 90*(4), 2154-2161.

Hasson, A.S., Moore, C.M., & Smith, I.W. (1998). The fluorine atom initiated oxidation of CF_3CFH_2 (HFC-134a) studied by FTIR spectroscopy. *International Journal of Chemical Kinetics, 30*(8), 541-554.

Hubrich, C., & Stuhl, F. (1980). The ultraviolet absorption of some halogenated methanes and ethanes of atmospheric interest. *Journal of Photochemistry*, *12*(2), 93-107.

Kelly, T., Bossoutrot, V., Magneron, I., Wirtz, K., Treacy, J., Mellouki, A., Sidebottom, H., & Le Bras, G. (2005). A kinetic and mechanistic study of the reactions of OH radicals and Cl atoms with 3, 3, 3-trifluoropropanol under atmospheric conditions. *The Journal of Physical Chemistry A, 109*(2), 347-355.

Kerr, J.A., & Calvert, J.G. (1965). The formation and decomposition reactions of the acetyle radical and the heat of formation of the acetyl radical. *The Journal of Physical Chemistry, 69*(3), 1022-1029.

Kerr, J.A., & Parsonage, M.J. (1976). *Evaluated kinetic data on gas phase hydrogen transfer reactions of methyl radicals*. Butterworth, London.

Kerr, J.A., & Sheppard, D.W. (1981). Kinetics of the reactions of hydroxyl radicals with aldehydes studied under atmospheric conditions. *Environmental Science & Technology, 15*(8), 960-963.

Kovacevic, G., & Sabljic, A. (2017). Atmospheric oxidation of halogenated aromatics: comparative analysis of reaction mechanisms and reaction kinetics. *Environmental Science: Processes & Impacts, 19*(3), 357-369.

Laidler, K.J. (1969). *Theory of chemical reaction rates*. McGraw-Hill, New York.

Lee, C., Yang, W., & Parr, R.G. (1988). Development of the Colle-Salvetti correlation-energy formula into a functional of the electron density. *Physical Review B, 37*(2), 785. https://doi.org/10.1103/PhysRevB.37.785.

Libuda, H., Zabel, F., Fink, E., & Becker, K. (1990). Formyl chloride: UV absorption cross sections and rate constants for the reactions with chlorine atom and hydroxyl radical. *Journal of Physical Chemistry, 94*(15), 5860-5865.

Liu, J.Y., Li, Z.S., Wu, J.Y., Wei, Z.G., Zhang, G., & Sun, C.C. (2003). Theoretical study and rate constant calculation of the CH 2 O+ CH 3 reaction. *The Journal of Chemical Physics*, *119*(14), 7214-7221.

Liu, M.T., & Laidler, K. (1968). Elementary processes in the acetaldehyde pyrolysis. *Canadian Journal of Chemistry, 46*(4), 479-490.

Liu, X., Spiekermann, K.A., Menon, A., Green, W.H., & Head-Gordon, M. (2025). Revisiting a large and diverse data set for barrier heights and reaction energies: best practices in density functional theory calculations for chemical kinetics. *Physical Chemistry Chemical Physics*, *27*(25), 13326-13339.

Ma, F., Xie, H.B., & Chen, J. (2018). Benchmarking of DFT functionals for the kinetics and mechanisms of atmospheric addition reactions of OH radicals with phenyl and substituted phenyl-based organic pollutants. *International Journal of Quantum Chemistry, 118*(10), e25533. https://doi.org/10.1002/qua.25533.

Ma, Y., & Li, B. (2025). A comparative study of kinetic and thermodynamic mechanisms of XH_4+ H→ XH_3+ H_2 reaction (X= Si, Ge, and Sn). *AIP Advances, 15,* 075138. https://doi.org/10.1063/5.0279640.

Mahmood, A., & Longo, R.L. (2016). Structural and relative energy assessments of DFT functionals and the MP2 method to describe the gas phase methylation of nitronates:$[R^1R^2CNO_2]^-$+ CH_3I. *Physical Chemistry Chemical Physics, 18*(25), 17062-17070.

Manthorne, K.C., & Pacey, P.D. (1978). The reaction of methyl radicals with formaldehyde in dimethyl ether pyrolysis. *Canadian Journal of Chemistry, 56*(10), 1307-1310.

Mardirossian, N., & Head-Gordon, M. (2016). How accurate are the Minnesota density functionals for noncovalent interactions, isomerization energies, thermochemistry, and barrier heights involving molecules composed of main-group elements?. *Journal of Chemical Theory and Computation, 12*(9), 4303-4325.

Mendes, J., Zhou, C.-W., & Curran, H.J. (2014). Theoretical chemical kinetic study of the H-atom abstraction reactions from aldehydes and acids by H atoms and OH, HO_2, and CH_3 radicals. *The Journal of Physical Chemistry A, 118*(51), 12089-12104.

Montzka, S., Reimann, S., Engel, A., Krüger, K., O'Doherty, S., Sturges, W., Blake, D.R., Dorf, M., Fraser, P.J., Froidevaux, L., Jucks, K., Kreher, K., Kurylo, M.J., Mellouki, A., Miller, J., Nielsen, O.J., Orkin, V.L., Prinn, R.G., Rhew, R., Santee, M.L., Verdonik, D.P. (2011). *Scientific assessment of ozone depletion: 2010, global ozone research and monitoring project – report no. 52*, World Meteorological Organization, Geneva, Switzerland.

Mora-Diez, N., & Boyd, R.J. (2002). A computational study of the kinetics of the NO_3 hydrogen-abstraction reaction from a series of aldehydes (XCHO: X= F, Cl, H, CH_3). *The Journal of Physical Chemistry A, 106*(2), 384-394.

Mora-Diez, N., Alvarez-Idaboy, J.R., & Boyd, R.J. (2001). A quantum chemical and TST study of the OH hydrogen-abstraction reaction from substituted aldehydes: FCHO and ClCHO. *The Journal of Physical Chemistry A, 105*(39), 9034-9039.

Nguyen, H.T., & Nguyen, X.S. (2018). Theoretical study of the addition and hydrogen abstraction reactions of the methyl radical with formaldehyde and hydroxymethylene. *Journal of the Serbian Chemical Society, 83*(10), 1113-1122.

Niki, H., Maker, P., Savage, C., & Breitenbach, L. (1980). An FTIR study of the Cl atom-initiated oxidation of CH_2Cl_2 and CH_3Cl. *International Journal of Chemical Kinetics, 12*(12), 1001-1012.

O'Doherty, S.J., & Carpenter, L.J. (2007). Halogenated volatile organic compounds. In: Koppmann, R. (ed) *Volatile Organic Compounds in the Atmosphere* (pp. 173-220). Wiley-Blackwell, Hoboken, New Jersey.

Park, H., Kim, Y., & Sim, E. (2019). Understanding DFT calculations of weak interactions: density-corrected density functional theory. *Journal of the Korean Chemical Society, 63*(1), 24-28.

Peng, C., & Schlegel, H.B. (1993). Combining synchronous transit and quasi-newton methods to find transition states. *Israel Journal of Chemistry, 33*(4), 449-454.

Ruscic, B., Pinzon, R.E., Morton, M.L., von Laszevski, G., Bittner, S.J., Nijsure, S.G., Amin, K.A., Minkoff, M., Wagner, A.F. (2004). Introduction to active thermochemical tables: several "key" enthalpies of formation revisited. *The Journal of Physical Chemistry A, 108*(45), 9979-9997.

Ruscic, B., Pinzon, R.E., Von Laszewski, G., Kodeboyina, D., Burcat, A., Leahy, D., Montoy, D., & Wagner, A.F. (2005). Active thermochemical tables: thermochemistry for the 21st century. *Journal of Physics: Conference Series*. *16*, 561. https://doi.org/10.1088/1742-6596/16/1/078.

Sanhueza, E., & Heicklen, J. (1975). Chlorine-atom sensitized oxidation of dichloromethane and chloromethane. *The Journal of Physical Chemistry, 79*(1), 7-11.

Scollard, D., Treacy, J., Sidebottom, H., Balestra-Garcia, C., Laverdet, G., LeBras, G., MacLeod, H., & Teton, S. (1993). Rate constants for the reactions of hydroxyl radicals and chlorine atoms with halogenated aldehydes. *The Journal of Physical Chemistry, 97*(18), 4683-4688.

Su, Y., & Francisco, J.S. (1995). A computational study of the reaction between methyl radicals and HXCO (where X= H and F). *Chemical Physics Letters, 236*(1-2), 162-166.

Tapia, O., & Goscinski, O. (1975). Self-consistent reaction field theory of solvent effects. *Molecular Physics, 29*(6), 1653-1661.

Truhlar, D.G., & Pliego Jr, J.R. (2006). Transition state theory and chemical reaction dynamics in solution. In: Mennucci, B., & Camm, R. (eds) *Continuum Solvation Models in Chemical Physics: Theory and Application* (pp. 339-366). Wiley. Chichester.

Truong, T., & Duncan, W. (1999). A reaction class approach for modeling gas phase reaction rates. *Physical Chemistry Chemical Physics, 1*(6), 1061-1065.

Varghese, J.J., & Mushrif, S.H. (2019). Origins of complex solvent effects on chemical reactivity and computational tools to investigate them: a review. *Reaction Chemistry & Engineering, 4*(2), 165-206.

Vijayakumar, S., & Wilmouth, D.M. (2021). Atmospheric fate of formyl chloride and mechanisms of the gas-phase reactions with OH radicals and Cl atoms. *Chemical Physics Letters, 777*, 138709.

Vohringer-Martinez, E., Hansmann, B., Hernandez, H., Francisco, J., Troe, J., & Abel, B. (2007). Water catalysis of a radical-molecule gas-phase reaction. *Science, 315*(5811), 497-501.

Volman, D.H., & Brinton, R.K. (1952). Reactions of free radicals with aldehydes. the reactions of methyl and t-butoxy radicals with acetaldehyde and acrolein. *The Journal of Chemical Physics, 20*(11), 1764-1768.

Wallington, T.J., & Hurley, M.D. (1993). Atmospheric chemistry of formyl fluoride: reaction with hydroxyl radicals. *Environmental Science & Technology, 27*(7), 1448-1452.

Wallington, T.J., Andersen, M.P.S., & Nielsen, O.J. (2017). Atmospheric chemistry of halogenated organic compounds. In: Barker, J.R., & Steiner, A.L. (eds) *Advances in Atmospheric Chemistry* (pp. 305-402). World Scientific, New Jersey.

Wallington, T.J., Hurley, M., Ball, J.C., & Kaiser, E.W. (1992). Atmospheric chemistry of hydrofluorocarbon 134a: fate of the alkoxy radical 1, 2, 2, 2-tetrafluoroethoxy. *Environmental Science & Technology, 26*(7), 1318-1324.

Wigner, E. (1932). On the quantum correction for thermodynamic equilibrium. *Physical Review, 40*(5), 749. https://doi.org/10.1103/PhysRev.40.749.

Wilmouth, D.M., Salawitch, R.J., & Canty, T.P. (2018). Stratospheric ozone depletion and recovery. In Török, B., & Dransfield, T. (eds) *Green Chemistry* (pp. 177-209). Elsevier. Boston.

Yasunaga, K., Kubo, S., Hoshikawa, H., Kamesawa, T., & Hidaka, Y. (2008). Shock-tube and modeling study of acetaldehyde pyrolysis and oxidation. *International Journal of Chemical Kinetics, 40*(2), 73-102.

Zokaie, M., Hashemi, S.R., & Saheb, V. (2021). Mechanism and kinetics of the reaction CH_3+CH_3CHO: ab initio semiclassical transition state theory study. *International Journal of Quantum Chemistry, 121*(4), e26468. https://doi.org/10.1002/qua.26468.